

DYNAMICS OF A LIQUID DROP IN A FLOWING IMMISCIBLE LIQUID

Stefano Guido ¹ and Francesco Greco ²

¹ Dipartimento di Ingegneria chimica, Università di Napoli “Federico II”

² Istituto per i materiali compositi e biomedici, CNR, Napoli
P.le V. Tecchio, 80 – 80125 Napoli, Italy

ABSTRACT

In this article we discuss the dynamics of a single drop immersed in an immiscible fluid with a given velocity field at infinity. Drop relaxation is also discussed. Newtonian and non-Newtonian fluid components are considered, to examine the effects of constitutive elasticity on drop deformation modes. Both experimental and theoretical results are reviewed. We illustrate in some detail three main issues of research of the last decade, namely, the exploitation of rheo-optical techniques, the study of large deformations and break-up, through numerical simulations, and the advancements in single drop theory for the case of non-Newtonian fluid components.

KEYWORDS: Single drop; Drop deformation; Drop break-up; Flow; Non-Newtonian fluids.

1. INTRODUCTION

Immiscible liquid-liquid suspensions, such as emulsions and polymer blends, are frequently encountered in a variety of applications, including, e.g., cosmetics and pharmaceuticals design, food processing, and plastics technology [1, 2]. Many physical and rheological properties of these systems are strongly dependent on morphology, i.e., size and shape of the dispersed phase inclusions. Morphology control is therefore of great importance, and can often be achieved by proper setting of the flow conditions experienced during processing. It is then understood how investigating the fluid-dynamic behaviour of these systems can be relevant for practical purposes. The fluid-dynamic problem is, of course, significantly simplified in the case of “dilute” suspensions, where drop-drop interactions can be neglected, and coalescence does not take place.

In this review article, we consider the idealized, but basic situation of a single drop in well-controlled flow conditions, a subject which has received much attention in the scientific literature, from both the theoretical and the experimental side, starting from the pioneering work of Taylor in the 1930s [3, 4]. This subject has been summarized in two well-known reviews by Rallison in 1984 [5] and Stone in 1994 [6].

Quite recently, another review article on microstructural evolution in blends has been authored by Tucker and Moldenaers [7], but the main emphasis is there on concentrated systems and their rheological properties. Here instead we focus on single drop dynamics, leaving aside the rheology of the dilute system as a whole. Concerning flow fields, only shear and elongation will be considered, which however encompass the majority of the works reported in the literature. Within this context, our aim is to describe and discuss what we believe are the main achievements of the last decade, although reference to earlier works will be made when necessary.

Among these achievements, we first mention the progress in the experimental techniques used to obtain well-controlled flow fields and to visualize a single drop during its motion. It is now a common practice to implement flow control through computer-assisted operation of motorized devices, e.g., linear and rotary stages, and to image drop shape by video enhancement (including microscopy) and processing techniques. This allows for a very precise characterization of drop shape, even at small deformations and/or under transient conditions. Another area of significant advancements in the last ten years is that of numerical simulations of the single drop fluid-dynamics, at least for the case where the two fluid components are Newtonian. Both by exploiting the steadily increasing computing power and memory resources, and by clever adoption of new integration schemes, a fine resolution of drop interface has been achieved, thus allowing one to deal with the case of high and extreme deformations. It has been so possible to gain a good understanding of drop break-up, a phenomenon that had been elusive for years. Third, the fluid-dynamic theory of the single drop for non-Newtonian fluid components has been developed in the limit of small deformations, and relevant non-dimensional parameters have been identified. This provides a framework to interpret experimental results, including those from much earlier works, and to suggest new experiments to be performed, in order to evaluate viscoelastic effects. This is an active area of research, also in view of the fact that many liquid-liquid suspensions of practical relevance are made up of non-Newtonian components.

The article is organized as follows. A major division of the text in two parts is made, dealing with fully Newtonian and with non-Newtonian systems. Each part starts with a section on theoretical aspects, to introduce the relevant quantities and the non-dimensional parameters to be used in the following. The first part on Newtonian systems is then composed of four sections, devoted to stationary drop shapes, break-up, retraction, and transient behaviour, respectively. On the other hand, due to the limited experimental evidence available on non-Newtonian systems, the second part is simply divided into two sections, dealing with shear and elongational flows. The article is closed by a short section where a few concluding remarks are given.

2. NEWTONIAN SYSTEMS

2.1 Mathematical Background for the Newtonian Case

In this section, we briefly illustrate the fluid-dynamics of the drop problem with Newtonian component fluids, and describe how the governing dynamical equations have been tackled to get asymptotic (“slow flow”) and numerical results. Also, we sum up some recent “phenomenological” models that, leaving aside the

possibility of obtaining exact solutions of the complete fluid-dynamics, nevertheless have the merit of giving useful predictions with only a modest mathematical effort. In a later section, this same scheme of presentation will be taken up again for the much more complex case with non-Newtonian component fluids.

The dynamics of a fluid drop (of rest radius R_0) suspended in a second fluid that is itself in motion, usually in response to a prescribed evolution of far-field boundary conditions, is patently quite a difficult subject. When the drop under study is sufficiently small with respect to any typical dimension L of its ambient of motion, i.e., when $R_0 \ll L$, the “outer” dynamics is dictated by the undisturbed flow. In the simplest case, one assumes that the drop is suspended in an unbounded fluid, and the undisturbed velocity field “at infinity” is linear, so that $\mathbf{v} \rightarrow \mathbf{L}^{(\infty)} \cdot \mathbf{r}$, with $\mathbf{L}^{(\infty)}$ the imposed velocity gradient, a function of time in the general case. Another usual assumption is that the Reynolds number of the fluid motion governing the deforming drop is low, i.e., $Re \equiv \rho |\mathbf{L}^{(\infty)}| R_0^2 / \eta \ll 1$, with ρ and η the density and viscosity, respectively, of the external fluid. Notice in this regard that, in view of the condition $R_0 \ll L$, the Reynolds number appropriate to the motion of the system as a whole needs not to be small: local creeping flow may also exist in rapid ambient flows. Such possibility is not considered in this review, however. Finally, to maintain the simplest possible situation, external and buoyancy forces are assumed negligible, the two fluids are taken to be incompressible and mutually immiscible, and isothermal conditions hold.

With all these simplifying assumptions, the single drop problem with Newtonian component fluids is described through the continuity and Navier-Stokes equations (the latter in the creeping flow limit), as:

$$\nabla \cdot \mathbf{v} = 0, \quad -\nabla P + \eta \nabla^2 \mathbf{v} = \mathbf{0}, \quad \dots\dots\dots(1)$$

$$\nabla \cdot \mathbf{v}_d = 0, \quad -\nabla P_d + \eta_d \nabla^2 \mathbf{v}_d = \mathbf{0},$$

for the external and internal fields, respectively. (From now on, all quantities referring to the inner fluid will be denoted with the sub-index d). The boundary conditions at infinity are simply $\mathbf{v} \rightarrow \mathbf{L}^{(\infty)} \cdot \mathbf{r}$, as discussed above, and $P \rightarrow P^{(\infty)}$, as $\mathbf{r} \rightarrow \infty$. In view of incompressibility, the constant pressure $P^{(\infty)}$ can be taken to be zero with no loss of generality. By describing now the drop surface at time t as $F(\mathbf{R}, t) = 0$ (\mathbf{R} is the position vector of a point at the interface), and with $\mathbf{N} = \nabla F / |\nabla F|$ the external normal to the drop surface, the interfacial boundary conditions read:

$$\mathbf{v} = \mathbf{v}_d, \quad \dots\dots\dots(2)$$

$$-\mathbf{v} \cdot \mathbf{N} = \frac{1}{|\nabla F|} \frac{\partial F}{\partial t}, \quad \dots\dots\dots(3)$$

$$\sigma \mathbf{N} \nabla \cdot \mathbf{N} = (P_d - P) \mathbf{N} + 2(\eta \mathbf{D} - \eta_d \mathbf{D}_d) \cdot \mathbf{N}, \quad \dots\dots\dots(4)$$

with $\mathbf{D} \equiv (\mathbf{L} + \mathbf{L}^T) / 2$ the local strain rate of the outer fluid at the interface (and \mathbf{D}_d that of the inner fluid), and σ the interfacial tension. In writing equation (4) for the

interfacial stress jump, the further assumption was made that the interfacial tension is constant, hence so-called “Marangoni motions” [8] are excluded.

The above equations are non-dimensionalized as follows. The only characteristic length of the problem is the rest drop radius R_0 , which is then the unit length. We choose that stresses are scaled with the interfacial stress σ/R_0 . Notice that, accordingly, external and internal velocities are scaled differently, by using σ/η , and σ/η_d , respectively. Notice also that the resulting time scale is the so-called *emulsion time* $\tau_{em} \equiv R_0\eta/\sigma$, the only intrinsic time existing in the Newtonian case. With these choices, all the above equations stay unaltered, with the constitutive parameters η , η_d , and σ gone, except for equation (2) at the interface, which becomes $\mathbf{v} = \mathbf{v}_d/\lambda$, with $\lambda \equiv \eta_d/\eta$ the viscosity ratio. The velocity boundary condition at infinity becomes:

$$\mathbf{v} \rightarrow \frac{R_0\eta|\mathbf{L}_{DIM}^{(\infty)}|}{\sigma} \mathbf{L}^{(\infty)} \cdot \mathbf{r} \quad \dots\dots\dots(5)$$

($|\mathbf{L}_{DIM}^{(\infty)}|$ is the *dimensional* magnitude of the imposed velocity gradient at infinity.) The non-dimensional group appearing in equation (5) is the well-known *capillary number* $Ca \equiv R_0\eta|\mathbf{L}_{DIM}^{(\infty)}|/\sigma$, the ratio of viscous to interfacial stresses. Note that, equivalently, we can look at the capillary number as the Deborah number [9] for the drop problem with Newtonian component fluids, since $Ca \equiv \tau_{em}/(|\mathbf{L}_{DIM}^{(\infty)}|^{-1})$ is the ratio of the intrinsic to the external time. The two non-dimensional numbers λ and Ca fully parameterize single drop dynamics in the Newtonian case.

The major source of difficulty in solving the complete fluid-dynamic problem is in the fact that the interfacial boundary conditions to be satisfied, i.e., equations (2)-(4), are assigned on the surface of the deforming drop, which is itself unknown. Pressure and velocity fields, inside and outside the drop, and drop shape must all be determined simultaneously, which is a very complex 3D moving boundary problem. It is not surprising then that analytic results have only been obtained under limiting conditions, when drop deformation from the unperturbed spherical shape is small at all times. In fact, small drop deformations occur in two cases, either for very large values of the ratio λ (i.e high viscosity drops do not deform), or for small capillary number Ca (i.e interfacial forces are dominant). In the latter case, the so-called “weak flow limit”, Ca is the obvious expansion parameter to be adopted in a perturbation procedure (inclusive of a “domain perturbation” technique [10], whereby actual interfacial boundary conditions are projected to a virtual spherical interface). The first-order problem was solved long ago by Taylor [3, 4], who used a solution of the inertialess, Navier-Stokes equations, in terms of series of spherical harmonics. By adopting the same mathematical approach, several authors later attacked the second-order problem, which of course is algebraically much heavier. In the end, exact perturbative solutions were found up to second-order in Ca [11, 12].

Skipping all details of these Ca and Ca^2 solutions, we will instead report here a simple and compact perturbative result that has been obtained very recently [13], for steady-state situations, by reasoning as follows. At steady state, all the unknown fields

(pressure, velocity, and drop shape) must be completely determined by the “driving force” at infinity, i.e., by the imposed *constant* velocity gradient $\mathbf{L}^{(\infty)}$. On the other hand, we can write down the tensorial representations of these fields in terms of *time-dependent* $\mathbf{L}^{(\infty)}(\mathbf{t})$ (and $\dot{\mathbf{L}}^{(\infty)}(\mathbf{t})$), when an arbitrary rotation (or change of frame) is superposed on the steady flow. Because of rotational invariance requirements, however, tensor $\mathbf{D}^{(\infty)}(\mathbf{t})$ and the vorticity tensor $\mathbf{W}^{(\infty)}(\mathbf{t})$ will in fact appear, in place of tensor $\mathbf{L}^{(\infty)}(\mathbf{t})$. Thus, merely from rotational invariance, the tensorial representations of all unknown fields at any order in Ca are obtained at once. For the drop shape, up to second order in Ca, we get the deceptively simple expression:

$$\mathbf{R}(\mathbf{u}) = 1 + \text{CaTD}^{(\infty)} : \mathbf{u}\mathbf{u} + \text{Ca}^2 \left[s_1 \mathbf{D}^{(\infty)} \mathbf{D}^{(\infty)} : \mathbf{u}\mathbf{u}\mathbf{u}\mathbf{u} + s_2 \mathbf{D}^{(\infty)} \cdot \mathbf{D}^{(\infty)} : \mathbf{u}\mathbf{u} + s_3 \mathbf{D}^{(\infty)} : \mathbf{D}^{(\infty)} + s_4 (-\mathbf{W}^{(\infty)} \cdot \mathbf{D}^{(\infty)} + \mathbf{D}^{(\infty)} \cdot \mathbf{W}^{(\infty)}) : \mathbf{u}\mathbf{u} \right] \dots\dots\dots(6)$$

(\mathbf{u} is a unit vector identifying a direction in space), where the five scalar coefficients, T plus the four s_i , only depend on the viscosity ratio λ . Results such as that of equation (6), being rooted in invariance arguments and representation theorems only, are of wide generality: we will see later in this review how this kind of approach is relevant in the non-Newtonian case.

When leaving the small deformation limit, no general analytic solution is known, hence numerical simulations of the full fluid-dynamics come to the fore. True progress in this area, however, has only been obtained recently, by exploiting a different mathematical formulation than the one given by equations (1) to (4). Indeed, it can be shown that, for any given point \mathbf{R} of the drop surface, the velocity $\mathbf{v}(\mathbf{R})$ is given by [14]:

$$\mathbf{v}(\mathbf{R}) = \text{Ca} \frac{2}{1+\lambda} \mathbf{L}^{(\infty)} \cdot \mathbf{R} - \frac{1}{4\pi(1+\lambda)} \int_A \nabla \cdot \mathbf{N} \left(\frac{\mathbf{I}}{|\mathbf{X}|} + \frac{\mathbf{X}\mathbf{X}}{|\mathbf{X}|^3} \right) \cdot \text{NdA} + \frac{3}{2\pi} \frac{1-\lambda}{1+\lambda} \int_A \frac{\mathbf{X}\mathbf{X}\mathbf{X}}{|\mathbf{X}|^5} : \mathbf{v}\text{NdA} \dots\dots\dots(7)$$

In equation (7), \mathbf{I} is the unit tensor, $\mathbf{X}=\mathbf{R}-\mathbf{R}'$, with \mathbf{R}' a generic point of the drop surface, and the integrals are calculated (by varying \mathbf{R}') over the drop surface. Notice that, in general, the velocity field *and* the interface A depend on time. Equation (7) is called the “Boundary Integral” representation of the drop problem, and gives us a powerful method for computing creeping flows by solving an equation for functions that are defined over the boundary only. The important benefit is, of course, that the dimensionality of the computational problem is reduced by one unit: computing a 3D flow reduces to solving an integral equation over the 2D domain representing the boundaries. It should be emphasized, anyway, that solving equation (7) still requires considerable computational efforts. Less than a decade ago, supercomputers had to be used [15]. Quite recent improvements in computational codes (in the last five years, say) allows now for the use of commonly available workstations. Some details on this point will be given below.

We finally come to phenomenological models of drop dynamics, which have also been developed in the last few years. All of these models start from the assumption that the drop shape is ellipsoidal at all times (from which the nicknaming of “ellipsoidal models”). Roughly speaking, experiments show that an ellipsoidal approximation for the drop shape is tenable when $Ca \leq 1$ and $\lambda = O(1)$ (and also for $Ca = O(1)$ and $\lambda \rightarrow \infty$, i.e., for highly viscous drops). Close to break-up, the drop shape deviates from the ellipsoid, and, correspondingly, the models should fail. Be it as it may, the ellipsoidal shape assumption amounts to say that drop shape is always described by the equation $\mathbf{Q}(t) : \mathbf{R}\mathbf{R} = 1$, with $\mathbf{Q}(t)$ a second rank, symmetric, and positive definite tensor, the dynamics of which fully describes the drop dynamics. The prototypical ellipsoidal model [16] then gives the evolutive equation for tensor \mathbf{Q} as:

$$\frac{d\mathbf{Q}}{dt} + \left(-\mathbf{W}^{(\infty)} \cdot \mathbf{Q} + \mathbf{Q} \cdot \mathbf{W}^{(\infty)} \right) + a \left(\mathbf{D}^{(\infty)} \cdot \mathbf{Q} + \mathbf{Q} \cdot \mathbf{D}^{(\infty)} \right) = -\frac{f}{\tau_{em}} \left[\mathbf{Q} - g(\mathbf{Q}) \mathbf{I} \right] \tag{8}$$

(For the sake of clarity, we revert here to dimensional variables.) In equation (8), drop dynamics is ruled by the competing actions of flow-induced deformations and of relaxation towards a spherical shape, the former being driven by the flow field at infinity, the latter occurring with a characteristic time τ_{em} . Notice that the first two terms in the LHS of the equation constitute the well-known corotational time derivative [9]. The function $g(\mathbf{Q})$ in the RHS is needed to preserve drop volume at all times. Coefficients a and f are the model parameters. A simple determination of such coefficients is obtained by non-dimensionalizing equation (8), then by expanding in Ca , and by comparing the resulting first-order equation with the exact Taylor solution for the drop. (In Taylor dynamics, the drop is exactly an ellipsoid.) It so turns out that a and f only depend on λ . By retaining these coefficients in the full equation (8), drop dynamics is then specified for whatever intensity and history of the imposed flow field.

A number of ellipsoidal models has been presented, all of them based on the same general idea of equation (8), namely, the competition between flow and relaxation. In fact, all these phenomenological models are embodied in the following single expression:

$$\frac{dQ_{ij}}{dt} + \left(-W_{ik}^{(\infty)} Q_{kj} + Q_{ik} W_{kj}^{(\infty)} \right) + \left(D_{ik}^{(eff)} Q_{kj} + Q_{ik} D_{kj}^{(eff)} \right) = -\frac{1}{\tau_{em}} R_{ij} \tag{9}$$

In equation (9), an “effective” flow field tensor $D_{ij}^{(eff)}$ and a “relaxation tensor” R_{ij} do appear, which are different in different models. Indeed, various “derivations” of these tensors have been proposed, e.g., by combining elastic inclusion and slender body models [17], or through approximate solutions from the boundary integral equation [18]. The effective flow field tensor is always found to be linear in the rate of strain at infinity, i.e., $D_{ij}^{(eff)} = A_{ijkl} D_{kl}^{(\infty)}$. In the principal frame of reference of the

ellipsoid, tensors A_{ijkl} and R_{ij} are both found to depend on the three axes of the drop. In view of this (to some extent artificial) flexibility of equation (9), good performances are often achieved by these models, as will be detailed below.

2.2 Stationary Drop Shapes

As already mentioned in the Introduction, one of the significant advancements occurred in the last decade is the development of experimental apparati that enabled detailed observations of drop shape under well-controlled flow conditions. Video-enhancement techniques are commonly applied to increase image contrast and to improve the detection of drop shape. Such pre-conditioned images can be converted in arrays of digital values (pixels) and processed by applying image analysis techniques [19] to extract geometrical features describing drop shape. Computer-assisted operation of the flow devices is also employed, to ensure well-controlled kinematic conditions and to keep the deformed drop within the field of view during motion. In this section, stationary drop shapes will be considered, both in the case of shear and elongational flow.

2.2.1 Steady state shear

To generate a well-controlled shear flow and, at the same time, to allow for optical accessibility, several apparati have been devised. A parallel band instrument was originally built by Taylor [4], who observed drop shape along the vorticity axis of shear flow. Many authors later used the Couette geometry [20] to perform observations along the velocity gradient direction, too. Another popular device is the rotational plate and plate.

Recently, a sliding plate apparatus, with set-ups enabling both “lateral” and “top” views, has been developed [21]. In both set-ups, one plate is displaced with respect to the other by a 2-axis translating stage, driven by two computer-controlled stepper motors. Parallelism between the two plates is adjusted by exploiting the reflections of a laser beam from the plate surfaces. Temperature is measured *in situ* by immersing a fine wire thermocouple in the sample between the two plates. Observations are performed by using a transmitted light microscope equipped with a monochromatic CCD video camera and a motorized focus system. The microscope itself is mounted on a motorized stage, to follow the deforming drop during motion.

The drop is injected in the continuous phase by means of a tiny glass capillary. A micromanipulator is used for a precise positioning of the capillary inside the gap. Since the chosen drop diameter (around 50 μm) is at least ten times smaller than the gap (1-2 mm), wall effects can be safely neglected. Images are acquired during motion and archived for later analysis. Quantitative characterization of drop shape is performed by an automated image analysis procedure, based on an edge-detection algorithm.

Typical stationary drop images at low to moderate drop deformations are shown in figure 1a for the view along the vorticity axis, and in figure 1b for the view along the velocity gradient. In the images, the most significant (and readily

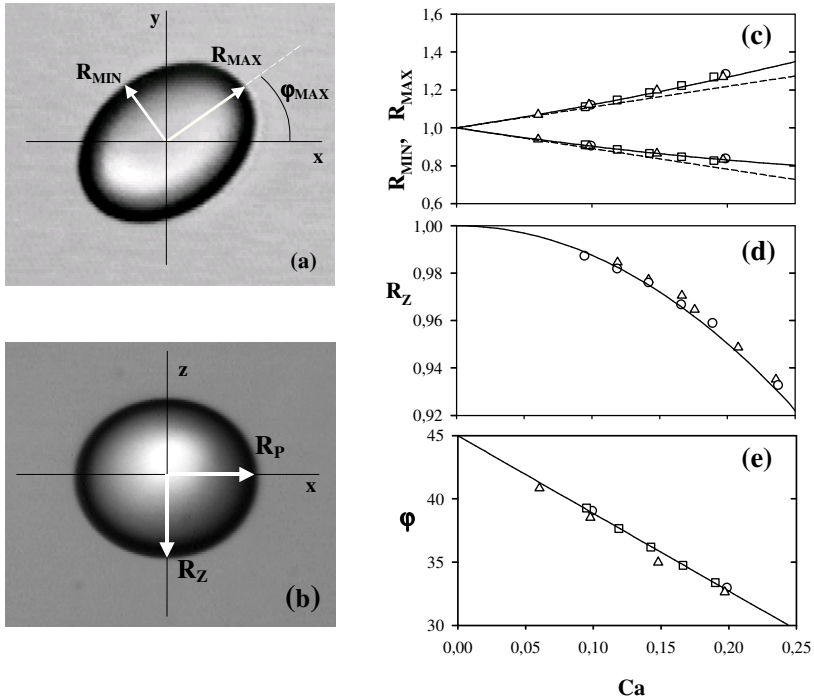


Figure 1: Left panel: side view (a) and top view (b) images of a drop during shear, and definition of the geometrical quantities used to describe drop shape. Right panel: plots of R_{MAX} , R_{MIN} , R_Z , and ϕ vs Ca at $\lambda = 1$. Data from [22], continuous and dashed lines refer to second and first order theory, respectively.

observable) geometric parameters are also shown, namely: i) (figure 1a) the maximum and minimum distances R_{MAX} and R_{MIN} of the contour from the drop centre, and the angle ϕ between R_{MAX} and the shear direction x in the lateral view; ii) (figure 1b) the maximum and minimum distances R_P and R_Z of the contour from the drop centre in the top view. (Notice that, contrary to R_P , the drop axis R_Z in the vorticity direction is unaffected by the projection.) In both views, the drop contour is very well approximated by an ellipse. Although calculations show that drop shape is not perfectly ellipsoidal already at order Ca^2 , it is apparent that the ellipsoidal approximation is a close description of drop shape up to moderate deformations. Hence, the three axes R_{MAX} , R_{MIN} and R_Z , and the angle ϕ provide a meaningful representation of drop shape.

As already stated in the introduction, the perturbative solution of the complete fluidodynamic problem is available up to second order in Ca . At steady state, the

expressions for the three main axes and the angle ϕ (as deduced from equation (6)) are in the form [13]:

$$R_{\text{MAX}} = 1 + \text{Ca} \frac{16 + 19\lambda}{16(1 + \lambda)} + \text{Ca}^2 F(\lambda) \quad \text{.....(10)}$$

$$R_{\text{MIN}} = 1 - \text{Ca} \frac{16 + 19\lambda}{16(1 + \lambda)} + \text{Ca}^2 F(\lambda) \quad \text{.....(11)}$$

$$R_z = 1 + \text{Ca}^2 G(\lambda) \quad \text{.....(12)}$$

$$\phi = \frac{\pi}{4} - \text{Ca} \frac{(16 + 19\lambda)(3 + 2\lambda)}{80(1 + \lambda)} \quad \text{.....(13)}$$

(with F and G known functions of λ). The peculiar expressions for the axes R_{MAX} and R_{MIN} should be noticed, with one and the same second-order contribution in both equations (10) and (11). This result leads to noteworthy consequences, to be discussed below. Also, it should be noticed that the R_z -axis only deviates from the rest radius R_0 at second order in Ca. Finally, notice that the orientation angle is predicted from second-order theory to be linear in Ca (first-order theory merely gives $\phi = 45^\circ$).

Experimental data obtained through the sliding plate apparatus already described are in excellent agreement with predictions from equations (10)-(13) [22]. This is shown in figure 1c, d, e, where data refer to a silicone oil drop in a polyisobutylene matrix (both fluids being Newtonian in the experimental range investigated), at a viscosity ratio $\lambda = 1$. The solid and dashed lines in figure 1c correspond to second and first order theory, respectively. It is clearly seen how the quadratic theory gives the correct predictions, in spite of the fact that the capillary numbers explored are rather low. Needless to say, quadratic theory is definitely required for comparison with R_z and ϕ data (figures 1d and e).

A derived quantity often used to describe drop deformation (as determined in the lateral view) is $D \equiv (R_{\text{MAX}} - R_{\text{MIN}}) / (R_{\text{MAX}} + R_{\text{MIN}})$, the so-called deformation parameter, originally introduced by Taylor. From equations (10), (11), the deformation parameter up to second order in Ca turns out to be:

$$D = \text{Ca} \frac{16 + 19\lambda}{16(1 + \lambda)} \quad \text{.....(14)}$$

i.e., deviations from linear theory can only occur at third order (at least) in Ca. Thus, the linear equation (14) remains valid as far as second order theory is valid. This result is fully confirmed from data [22]. Steady state measurements of D, together with equation (14), therefore provide an accurate determination of the interfacial tension σ between drop and matrix fluids. Incidentally, notice that the dependence from λ in equation (14) is very weak, which is of help in determining reliable values for the interfacial tension with this method.

It is well known that drop shape and orientation are strongly affected by the viscosity ratio, thus extensive studies for a wide range of λ are in order. As an example, in figure 2, taken from Jackson and Tucker [17], classical measurements by

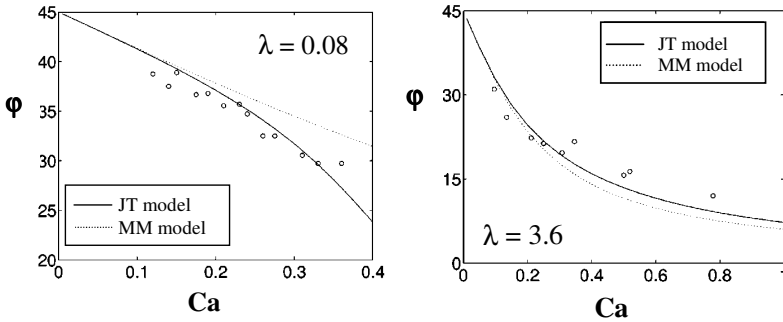


Figure 2: The orientation angle ϕ as a function of the capillary number Ca at $\lambda = 0.08$ and 3.6 (adapted from Jackson and Tucker [17]).

Torza *et al.* [20] of the orientation angle vs. Ca are reported, for $\lambda = 0.08$ and 3.6 . Clearly, the dependence of the angle on Ca is much stronger in the high viscosity ratio case, where a tendency to a plateau is also observed. Figure 2 also shows that the general features displayed by the experiments are well captured by ellipsoidal models. The use of such phenomenological models seems appropriate here, given the rather extended range of capillary number explored in the experiments. In fact, for the high viscosity ratio case $\lambda = 3.6$, data show that the linear dependence of ϕ on capillary number predicted by equation (13) is at most valid up to $Ca = 0.2$.

When going to high capillary numbers, and to correspondingly large drop deformations, the drop at steady state is no longer representable by an ellipsoid, and more complex shapes (e.g., sigmoidal in the shear plane [4]) are observed, depending on the viscosity ratio. In such situations, numerical simulations of the complete fluidodynamics are the only available general tool. In this field, the most significant advancement in the last decade has been the extensive application of boundary integral methods. In particular, the fully 3D problem (including shear flow) has been tackled in recent years, whereas only axisymmetric and/or equiviscous situations had been previously solved [5].

The challenging boundary integral simulation of the shear flow case has been pioneered by Pozrikidis and co-workers [15]. In order to resolve drop surface with sufficient accuracy even for highly deformed configurations, these authors had to deal with a rather large number of “marker” points, a situation that could be handled at the time only by using a supercomputer. Similar computationally heavy studies have been undertaken by Uijttewaal and Nijhof [23]. In both works, good agreement with experimental results was found. For example, the above reported data by Torza *et al.* on the orientation angle ([20], see figure 2) are well reproduced by simulations.

Numerical resolution in these studies is set by the number of markers used to discretize the initial undeformed spherical surface. In turn, discretization is limited by

available computational facilities. A way out of this limitation is to allow the number of nodes on the mesh to vary between the time steps. In other words, the surface mesh can be locally restructured to maintain uniform resolution of the local curvature on the drop surface, through a so-called “adaptive mesh” algorithm. Boundary integral simulations with adaptive discretization of the drop interface were performed by Loewenberg and co-workers [24]. In figure 3, calculated stationary drop shapes in shear flow are shown from a lateral view, at two different viscosity ratios, for capillary numbers just below the critical values for break-up. Notice how the grid density is higher in the regions at high curvature, near to the drop ends. It is apparent that the adaptive mesh algorithm is a powerful tool to study extreme deformations. With this algorithm, for the first time, the break-up phenomena become computationally accessible (see the drop break-up section).

2.2.2 Steady state elongation

Extensive experimental studies of planar elongational flows have been made possible in the last two decades by a new implementation of the “four-roll mill” apparatus, a device invented by Taylor in the 1930s [4]. This device produces a good approximation to a planar linear flow in the region between the four rollers, as sketched in figure 4, with a stagnation point located centrally between the rollers for any of the possible flows. The α parameter is representative of the relative weight of the rate of strain and vorticity tensors, as shown by the expression of the velocity gradient:

$$\nabla \mathbf{v} = \frac{|\mathbf{L}^{(\infty)}|}{2} \begin{bmatrix} 1 + \alpha & 1 - \alpha & 0 \\ -1 + \alpha & -1 - \alpha & 0 \\ 0 & 0 & 0 \end{bmatrix} \dots\dots\dots(15)$$

Equation (15) is written in the frame of reference adopted in figure 4. α can be varied by adjusting roller speed and direction of rotation. It should be remarked that, although in principle any value of α is attainable ($|\alpha| \leq 1$), shear flow ($\alpha = 0$) cannot be actually generated with satisfactory accuracy in the four-roll mill.

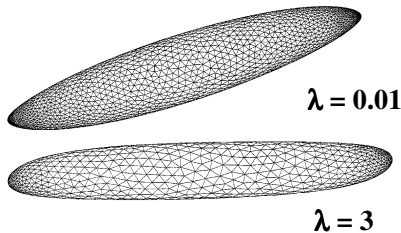


Figure 3: Stationary drop shapes in shear flow calculated by adaptive mesh boundary integral simulations at $\lambda = 0.01$ (top) and 3 (bottom).

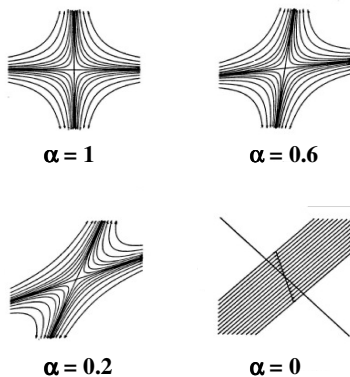


Figure 4: Linear flow fields in the four roll mill apparatus (adapted from Bentley and Leal [25]).

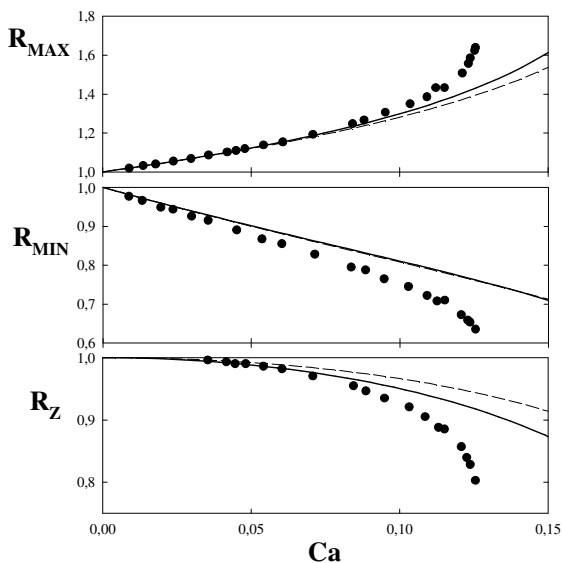


Figure 5: The three drop axes vs Ca under planar elongational flow at $\lambda = 0.7$. Data from Hu and Lips [26], ellipsoidal model predictions by Maffettone and Greco [27].

In operating the device, the drop should be placed at the stagnation point, so as to remain fixed for whatever imposed flow field. Unfortunately, however, the stagnation point of the flow is not a stable position, a difficulty that has hindered for many years the use of the four-roll mill. This difficulty has been overcome in 1986 by Bentley and Leal [25], who developed a computer-controlled feedback system to keep the drop in place. The system is based on a video camera interfaced to a computer, which allows online detection of drop position and continuous driving of the stepper motors to adjust rollers speed and direction.

For hyperbolic elongational flow ($\alpha = 1$), an extensive set of drop deformation data has been recently provided by Hu and Lips [26]. They used a miniaturized version of the four-roll mill apparatus, with two video cameras to simultaneously image drop shape in both the elongational plane and the neutral plane xz . A derivative edge detection algorithm was implemented to identify drop contours in both views. Temperature in the flow cell was measured by a thermocouple and controlled by a water-jacket system.

While a wide range of viscosity ratios ($10^{-4} - 10^2$) and capillary numbers (up to break-up) has been explored by Hu and Lips, we only report here in figure 5 a representative set of data for the drop axes, with $\lambda = 0.7$. (Obviously, drop orientation is here fixed along the elongational direction, by symmetry.) In the same figure, a comparison with predictions from two ellipsoidal models [27] is also given. As expected, good agreement with data is found up to moderate values of Ca , while progressively increasing deviations occur when approaching break-up, where drop shape presumably differs from an ellipsoid.

Concerning planar elongational flows with $\alpha \neq 1$, an extensive set of data has been reported by Bentley and Leal [25]. The shape parameters measured by these authors are the deformation parameter D (in the elongational plane) and the angle ϕ between the major drop axis and the direction at $+45^\circ$ with respect to the frame of reference of figure 4. In figure 6, as an example, data at $\lambda = 0.12$ and for two values of α (0.2 and 1) are shown. Notice how, by increasing α , the flow field becomes more effective in deforming the drop, a feature that is in fact observed at any value of λ . In figure 6, predictions from the Maffettone-Minale ellipsoidal model [16] are also shown, and good agreement is found in this case (agreement is worse at higher λ).

For the planar elongational case, as a matter of fact, numerical simulations of drop shape are not available. On the other hand, several boundary integral simulations have been performed for the case of uniaxial elongation, even up to break-up [24, 28, 29]. Indeed, in axisymmetric situations drop surface is specified by a curve, and this leads to a significant simplification of the governing dynamic equations. On the experimental side, pure uniaxial elongation is quite difficult to obtain. We are aware of only one set of data of drop deformation in such a flow field, reported by Delaby *et al.* [30]. This work, however, deals with a transient uniaxial elongation, and will be discussed in a later section.

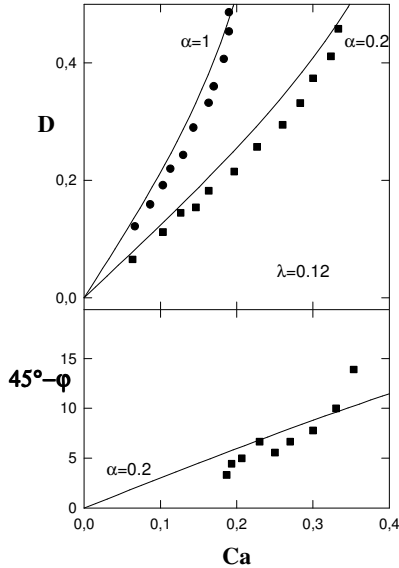


Figure 6: Drop deformation and orientation (in the frame of reference of figure 4) for two values of α [24]. Data from Bentley and Leal [25], predictions from Maffettone and Minale [16].

2.3 Drop Break-up

Drop break-up is a complex phenomenon. Although studies date back to Taylor, and much phenomenological evidence and approximate theoretical analyses have been collected through the years [6], a basic understanding has started only recently, even if limited to some histories of the imposed external flow and to $\lambda = O(1)$. This progress comes both from the finding of scaling laws near to break-up and from numerical results of advanced simulations. In this section, we only consider the case of break-up under steady external flows. In this situation, it is experimentally well known [31, 32] that stationary drop shapes (starting from the spherical configuration) are only reached up to a certain critical value Ca_{cr} of the capillary number, which depends on the type of imposed flow and on the viscosity ratio. Beyond Ca_{cr} a drop keeps deforming, until rupture occurs.

In figure 7, the shape evolution of an initially spherical drop in shear flow is shown, as calculated with adaptive mesh boundary integral simulations [24], for a slightly supercritical capillary number at $\lambda = 1$. The shapes shown in the sequence are very similar to those experimentally observed under close conditions. (A comparison between simulations and experiments is presented in figure 8.) Two features are

prominent in figure 7: i) the time evolution of drop shape undergoes a sudden acceleration towards the end of the sequence, when the drop takes a dumbbell form with two bulbous ends connected by a neck region; ii) in the very late stage of the sequence, the neck tends to pinch off near the bulbous ends, a clear indication that break-up is imminent. The inset in figure 7 shows the neck at the pinch-off region, which has been finely resolved through the adaptive mesh algorithm.

Despite such extreme resolving power, simulations per se cannot of course access the actual break-up event. To this end, some new insight into the fluidodynamics close to break-up should possibly come into play. This breakthrough has been made, recently, by Lister and Stone [33], based on the following ideas. Since, close to break-up, one can argue that the relevant length and time scales are order of magnitude less than those in the far field, it should be possible to perform a local analysis of the Navier-Stokes equations, to describe the evolution towards the “singularity”. Let us assume that in the pinch-off region, as break-up is approached, dynamics is governed by a viscous-capillary force balance, i.e. (in cylindrical

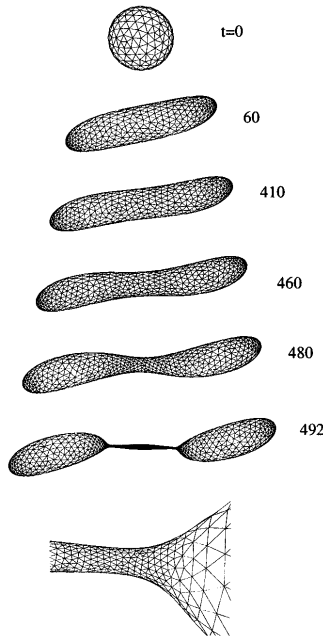


Figure 7: Numerical simulations of the shape evolution preceding breakup of an initially spherical drop in shear flow at $Ca = 0.42$ and $\lambda = 1$. Inset shows neck region at $t = 492$.

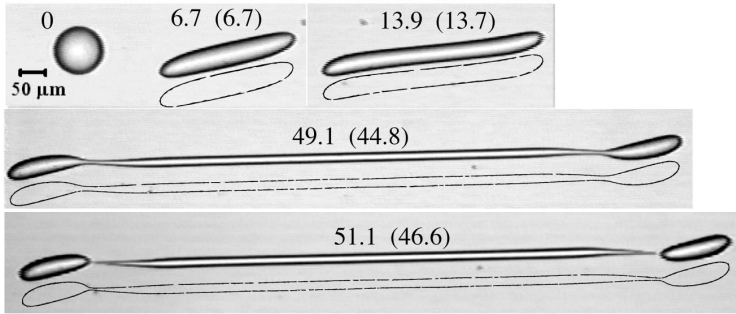


Figure 8: Drop images from shear experiments and contours from boundary integral simulations at different times (calculated values shown in parentheses) for $Ca/Ca_{cr} = 1.17$ and $\lambda = 1$ [35].

coordinates around the neck), $\eta \partial^2 v / \partial r^2 \approx \eta_d \partial^2 v / \partial z^2 \approx \sigma \partial r^{-1} / \partial r$, where v is the local velocity field. With ℓ the neck radius and ζ a characteristic axial length in the pinch-off region (see inset of figure 7), and with w a characteristic velocity, the viscous-capillary force balance is expressed by:

$$\begin{cases} \frac{\zeta}{\ell} \approx \sqrt{\frac{\eta_d}{\eta}} \\ w \approx \frac{\sigma}{\eta} \end{cases} \dots\dots\dots(16)$$

Equation (16) is the scaling law of the break-up process. Equation (16.1) expresses geometrical self-similarity, and equation (16.2) predicts the constancy of the velocity field near to the singularity. From equation (16), the axial length evolution when approaching the break-up time t_{cr} is ruled by $\zeta \equiv w(t_{cr} - t) \approx (\sigma/\eta)(t_{cr} - t)$, from which one gets the important relation:

$$\ell \approx \frac{\sigma}{\sqrt{\eta \eta_d}} (t_{cr} - t), \dots\dots\dots(17)$$

i.e., the characteristic radius ℓ thins linearly with time to break-up. As a check of the consistency of the initial assumption, notice that, based on the just illustrated results, the inertial force evolution is locally given by $\rho w^2/d \propto (t_{cr} - t)^{-1}$ (d is either ℓ or ζ), whereas viscous and capillary forces scale as $(t_{cr} - t)^{-2}$. Hence, near to break-up, local inertia is negligible, confirming the original ansatz.

The predicted neck thinning of equation (17), linear in time, has been actually observed in numerical simulations, both for uniaxial and shearing flows [33, 34, 24]. The break-up time t_{cr} is then obtained by extrapolating in time from simulations close to the pinch off event. In figure 8, lateral views of drop shapes from experiments and calculations under supercritical shearing conditions are compared [35], showing excellent agreement. In view of the experimental challenges and of the heavy calculations involved in such highly deformed situations, the slight differences in dynamics (the calculated evolution is 10% faster, at most, than in experiments) should be regarded as negligible.

The question remains on how to determine the critical capillary number itself. Experimental Ca_{cr} data have large scatter due to the uncertainty of assessing whether a drop is gradually breaking or eventually attaining a stationary configuration, when Ca is near to its critical value. The same difficulty applies to numerical computations. Indeed, it is observed that the time $\tau(Ca)$ required to reach a stationary shape diverges when approaching Ca_{cr} . To explain such behaviour, the following relationship has been proposed to hold in proximity of Ca_{cr} , based on heuristic arguments [34, 36]:

$$\tau(Ca) \propto \frac{1}{\sqrt{Ca_{cr} - Ca}} \quad \dots\dots\dots(18)$$

Equation (18) is in good agreement with numerical simulations and experiments. Hence, Ca_{cr} can be determined, by plotting τ vs Ca , as the abscissa of the vertical asymptote. In figure 9a [35], Ca_{cr} values determined by this procedure are compared to classical data by Grace, and agreement is good. Notice that, in figure 9a, calculated values of Ca_{cr} are only reported for the range $0.1 \leq \lambda \leq 2.5$. It is well known experimentally [31, 32] that, at very low values of λ , different break-up mechanisms occur, e.g., by tip streaming from pointed ends of the drop, which might be very difficult to simulate.

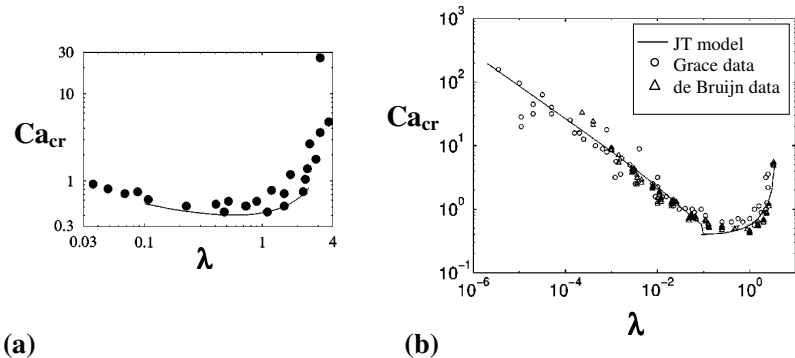


Figure 9: The critical capillary number in shear flow vs the viscosity ratio, from numerical simulations by Cristini *et al.* [35] (left plot) and the ellipsoidal model by Jackson and Tucker [17] (right plot). Data from Grace [31] and de Bruijn [32].

Although it is apparent that only refined numerical simulations can possibly catch the details of the break-up process, it is worth mentioning that nice predictions have been reported from simple phenomenological models. In figure 9b, the critical capillary number vs the viscosity ratio is reported, as calculated with the ellipsoidal model by Jackson and Tucker [17], and excellent agreement with data [31, 32] throughout seven decades of λ is found.

Going back to simulations, it should be mentioned that numerical techniques different from boundary integral methods have also recently been developed. We signal here the “volume of fluid” [37] and the “dissipative particle dynamics” [38] methods (the latter still being in a rather early stage of development). Both of these numerical methods provide a way of treating topological changes of the interface, hence post-break-up evolution can be monitored, and drop fragment distribution can be studied. Another advantage of these methods is that flow at finite Reynolds numbers can be simulated. Hence, for instance, the dependence of Ca_{cr} on the Reynolds number can be investigated [37].

In concluding this section, we would like to point out that the simple case of drop break-up under stationary flow (and at slightly supercritical conditions) has only been dealt with here. More complex break-up modes arise when the external flow is time-dependent, or during retraction. In such cases, a variety of effects has been observed, which are not even easy to file up, not to speak of providing a unifying interpretation. We quote from [39]: “The drop break-up process exhibits a substantial degree of sensitivity to the details of the deformation process. This is, in fact, quite disappointing in the sense that it seems to preclude any simple ‘scaling’ type arguments... that may aid in the evaluation and/or design of mixing devices”.

2.4 Drop Retraction

The phenomenon of drop retraction has received much attention in the literature in the last 15 years or so. Apart from the fact that complex and unexpected relaxation modes do appear, which *per se* provide a subject rich of features to be interpreted, experiments of drop retraction and their analysis have become a popular way to measure interfacial tension. Indeed, no special apparatus to impose a well-controlled flow field and/or a well-defined initial condition is required. As an example [40], in the case of polymer melts pairs, thin stripes of one polymeric material are cut in the solid state, and sandwiched between two moulded disks of the other component, then the temperature is raised up to fusion, and the retraction of the resulting stretched inclusion is monitored as a function of time (“imbedded fibre” method). The only experimental set-up required is therefore a suitable optics and an image analysis software to measure drop dimensions during retraction.

The imbedded fibre retraction method has been pioneered by Cohen and Carriere [40]. In figure 10, from their original paper, images of a retracting polystyrene fibre in a polymethylmetacrylate matrix are shown. Drop shape was modelled by Cohen and Carriere as a cylinder with hemispherical caps. Drop shape evolution was roughly described through a balance of Stokes and interfacial forces, i.e., $\zeta_S dR_{MAX}/dt = -\sigma dA/dR_{MAX}$, with R_{MAX} the drop major dimension, A the

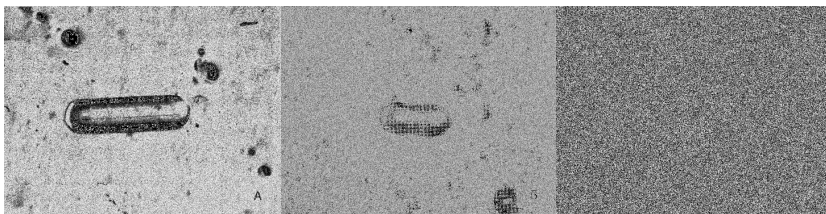


Figure 10: . Images of a retracting drop from Cohen and Carriere [40].

interfacial area, and $\zeta_S = \eta_{\text{eff}} R_{\text{eff}}$ a Stokes friction coefficient, where the effective radius R_{eff} is calculated through volume conservation, and the effective viscosity η_{eff} is a given combination of the viscosities of the component fluids. By solving the force balance equation, and by fitting the obtained solution $R_{\text{MAX}}(t)$ to data, the interfacial tension can then be estimated. A better estimate of interfacial tension can of course be obtained through a better description of drop shape evolution. Tjahjadi *et al.* [41] used boundary integral simulations to follow the relaxation of a modestly elongated drop back to a spherical shape, and proposed a procedure to obtain σ , based on an extended set of tabulated results (for viscosity ratios ranging from 0.01 to 10).

If the imbedded fibre is quite extended initially, it is well known [6] that a “varicose” instability develops during retraction, with an interfacial undulation of the fibre growing in time, until multi-break-up occurs, leading to the formation of a string of satellite drops. Although the multi-break-up mechanism is beyond the scope of this review, it should be mentioned that pre-break-up dynamics can, in fact, be exploited to estimate the interfacial tension (“breaking thread” method), hence a brief discussion seems at order here. The linear stability analysis, of an infinitely extended thread of a Newtonian liquid immersed in another Newtonian immiscible liquid, had been worked out by Tomotika in the 1930s [42]. He found that, when an initially infinitesimal sinusoidal perturbation is imposed on the liquid thread, a dominant distortion wavelength ξ develops, which grows at a rate $\tau = \tau_{\text{em}} \Omega(\lambda, \xi)$, with Ω a tabulated function. By measuring this growth rate, the interfacial tension, which is hidden into the emulsion time τ_{em} , can then be determined. The breaking thread method and Tomotika analysis have been used by Elemans *et al.* [43] in polymer/polymer systems. Indeed, in the case of polymer pairs, and provided that viscoelastic effects are negligible, this approach is especially convenient, since the high viscosities of polymers slow down the dynamics, and observations are easier. We finally mention that, similarly to the case of modestly deformed drop retraction, boundary integral simulations can be employed, to follow thread evolution well beyond the linear limit of Tomotika analysis. Tabulated results from simulations are again provided by Tjahjadi *et al.* [41].

The experimental observations of drop retraction reported so far have all been performed along the direction perpendicular to the enclosing surfaces. The merit of

giving a fully 3D characterization of the retracting drop goes to Takahashi and co-workers [44], who performed simultaneous top and lateral observations after shear step strain deformations. In figure 11a, the non-dimensional drop axes are shown as a function of time during relaxation, together with representative pictures of drop shapes (top view). It should be noticed how, in figure 11a, uniaxial symmetry appears to be recovered after a while, first through a rod-shaped and later through a dumbbell-shaped drop. (The latter configuration, which only appears at large enough strains, is also visible in the intermediate image of figure 10.) In particular, the uniaxial symmetry region corresponds to a minimum of the axis along the vorticity direction. Thereafter, in the late stage of the retraction, data are well described by a single exponential decay (see also below). Later data by Almusallam *et al.* [45] are reported in figure 11b, together with predictions from ellipsoidal models. Agreement is good, in spite of the fact that the ellipsoidal model obviously cannot reproduce the dumbbell shape of the drop at intermediate times.

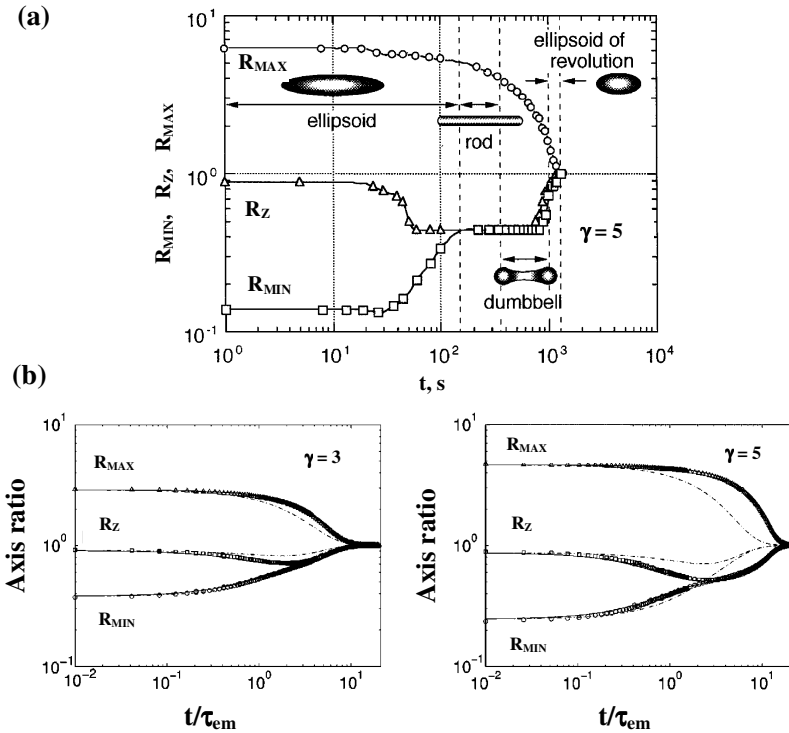


Figure 11: Drop relaxation after step shear. (a) Data and sketches of drop shape from Yamane *et al.* [44]; (b) Data from Almusallam *et al.* [45] and predictions from ellipsoidal models (dashed lines [16], solid lines [17]).

Since, as already stated, exact solutions of the fluidodynamic problem do exist for small deformations of the drop [12], the interfacial tension can also be obtained by fitting these theories to experimental data, even if quite accurate measurements are required to this purpose. Following this approach, Luciani *et al.* [46] obtained σ from top view experiments of drop retraction following a shear step strain, by using approximate values of the deformation parameter D (a quantity in fact pertaining to lateral projection of the drop). On the other hand, side view experiments of drop retraction after cessation of steady shear flow have been carried out by Guido and Villone [47], who compared their data to the exact first order formula (also used by Luciani *et al.*) for the time evolution of D :

$$D(t) = D_0 \exp\left(-\frac{40(\lambda+1)}{(2\lambda+3)(19\lambda+16)} \frac{t}{\tau_{em}}\right) \quad \dots\dots\dots(19)$$

D_0 is the steady-state value of the deformation parameter in shear flow (see equation (14)). The single exponential decay predicted by equation (19) is in excellent agreement with data, thus allowing for a precise determination of the interfacial tension. Similar results, for retraction after planar elongation, have been found by Hu and Lips, quite recently [26].

The description of drop shape by the deformation parameter does give only limited information about 3D evolution of the drop. For up to moderate deformations, a more accurate representation is provided by the three drop axes. These quantities have been analytically determined up to second order in the relevant expansion parameter (e.g., the capillary number Ca at steady state, see equations (10), (11) and (12)). For pre-shearing flows, of special relevance is the R_z axis, because it is directly measured in top view experiments. From theory, the R_z axis only deviates from R_0 at second order in Ca , and is predicted to follow a complex evolution during retraction (a sum of three exponentials), without going through a minimum, at variance with the high deformation case. In figure 12, the relaxation of R_z as a function of time is shown,

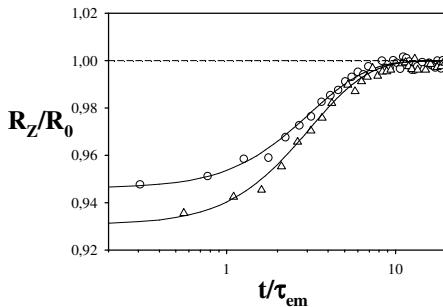


Figure 12: Relaxation of R_z as a function of time at $\lambda = 1$ [22]. Pre-shear capillary numbers $Ca=0.2$ (O) and $Ca=0.23$ (Δ). Continuous lines from second order small deformation theory.

at two pre-shear capillary numbers, together with the corresponding second order predictions, and excellent agreement is again found [22]. Thus, accurate R_z measurements can also be used to infer the interfacial tension.

We have illustrated how experiments of drop retraction combined with theoretical analyses are a simple and powerful tool to measure the interfacial tension. The application of this technique is widely documented in the literature, and variations on this theme continue to appear. Detailed comparisons of the results obtained from drop retraction with results from other methods are also available [48, 49], supporting the validity of the technique in a wide range of conditions.

2.5 Transients

Among the three categories of flow-field / drop-shape considered so far, we would like to go back to the case of break-up under externally imposed steady flow. Here, however, rather than on the near break-up dynamics, we focus on initial transients under highly supercritical conditions. Indeed, in such situations, unexpected and at least partially unexplained behaviours are encountered, exemplifying the complexities of drop dynamics.

Under shear flow, with $Ca \gg Ca_{cr}$ and $\lambda \ll 1$, it has been observed from top view experiments that the drop tends to “flatten” in the initial stage of its evolution. In other words, the R_z axis goes through a maximum before starting its decrease leading to break-up. Although, originally, this drop-widening phenomenon was observed for highly elastic polymeric materials [50], it has been recently documented for Newtonian fluid components too [51]. In figure 13, data are presented for such

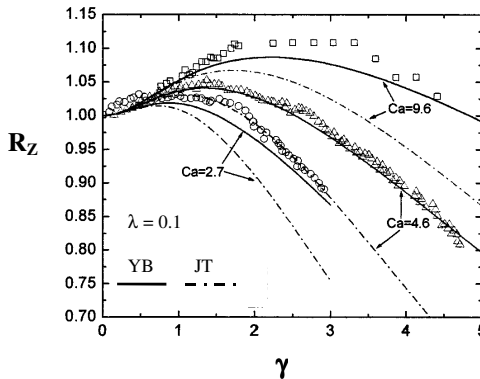


Figure 13: Transient drop widening in shear flow at supercritical capillary numbers for $\lambda = 0.1$. Data from [51], lines as predicted from ellipsoidal models [17, 18].

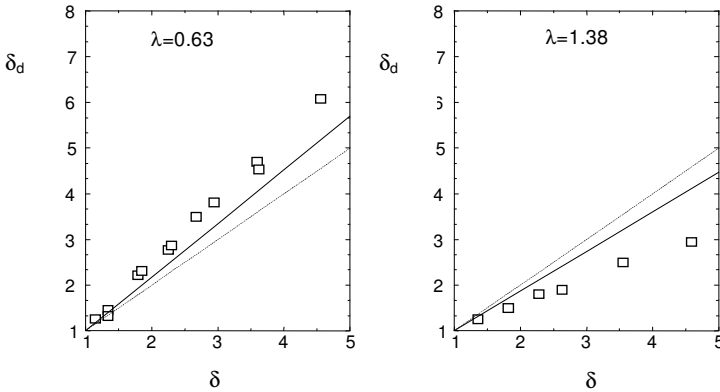


Figure 14: Drop elongational ratio δ_d vs the specimen elongational ratio δ (adapted from [30]). Dotted lines are for $\delta = \delta_d$.

Newtonian case, with $\lambda = 0.1$ (since $Ca_{cr} \approx 0.5$ at this viscosity ratio, the imposed capillary numbers in figure 13 correspond to highly supercritical conditions). In the same figure, predictions from ellipsoidal models [17, 18] are also reported, showing both qualitative and quantitative agreement with experiments. We mention that boundary integral simulations (not shown) are also in good agreement with data [51]. Notwithstanding these results, it should be frankly stated that the physical mechanism of transient drop widening is not really grasped. At the same time, it is apparent that the possibility of building up a “lamellar” morphology via an appropriate flow history is appealing for practical purposes, particularly if confirmed for concentrated systems.

Remaining in supercritical conditions, but going now to the elongational case, we are aware of only one set of data under applied uniaxial flow, reported by Delaby *et al.* [30]. Specimens were prepared by sandwiching a small number of inclusions into the matrix, and by melting. The so formed drops were individually identified by optical microscopy. An extensional rheometer allowing fast quenching of the stretched specimens was used. After reaching a prescribed deformation, a second microscopic observation of the stretched and quenched specimens made it possible to measure the deformation of each individual drop. A wide range of viscosity ratios ($10^{-3} < \lambda < 10$) was examined. Due to the high viscosity (around 10^6 Pa·s) of the polystyrene samples used as the matrix phase, the imposed capillary numbers were always at least one order of magnitude higher than Ca_{cr} , thus we are dealing here with a transient drop deformation. In figure 14, the drop elongational ratio δ_d vs the specimen elongational ratio δ is shown, for two viscosity ratios slightly below and above unity. The solid lines in the figure are from the equation $(\delta_d - 1)/(\delta - 1) = 5/(2\lambda + 3)$, deduced by Taylor in the small deformation limit. Given the high values of elongation attained in the experiments, deviations from Taylor predictions would in fact be expected here. Rather surprisingly, however, Delaby *et al.* demonstrated that Taylor formula applies

well to both very low and very high viscosity ratios. To justify these puzzling results, the authors proposed that the observed deviations at λ around unity are possibly due to viscoelastic effects. On the other hand, Delaby *et al.* data are seemingly in agreement with recent boundary integral simulations [29] of drop uniaxial elongation, for Newtonian fluids and in the limit of no interfacial tension ($Ca \rightarrow \infty$). Anyway, we stress that an actual comparison between data and simulations is not available.

Complex transients in drop shape are of course found when the imposed flow history is itself time-dependent. It is apparent that such history-dependent, and/or even non-rheometrical flow fields are relevant for applications, e.g., for mixing or dispersing devices. A remarkable case study of “realistic” fluido-dynamics has been presented quite recently by Feigl *et al.* [52]. These authors investigate an annular gap flow between two eccentric cylinders. (This flow geometry is an idealization of a rotor-stator dispersing device.) Finite element and numerical particle tracking techniques are used to obtain the flow field history along a particle trajectory, and from this history, boundary integral techniques are used to determine the deformation a drop would experience along this path. Thus, the key assumptions made in this approach are that the drop remains on a particle path, and that it is small compared to the length scale on which the velocity gradient varies spatially. Finally, experiments in an eccentric cylinder geometry are performed to verify the simulation procedure.

In figure 15, the schematic on the top right is the eccentric cylinder device as observed along its axis. The flow field in the annular gap is in the form:

$$\nabla \mathbf{v} = \begin{bmatrix} \dot{\epsilon} & \dot{\gamma} & 0 \\ 0 & -\dot{\epsilon} & 0 \\ 0 & 0 & 0 \end{bmatrix} \dots\dots\dots(20)$$

The velocity gradient in equation (20) is a local quantity, with $\dot{\epsilon}$ and $\dot{\gamma}$ the local elongational and shear rate, respectively. Notice that, in the general case, these quantities also depend on time. Calculated values of $\dot{\epsilon}$ and $\dot{\gamma}$ are plotted along a trajectory (shown on the top right) in the diagram on the top left of figure 15. As expected, the elongational rate goes through a pronounced maximum in the thinnest region of the annulus. When the calculated velocity gradient along a certain trajectory is now enforced in boundary integral simulations, the evolution of drop shape is obtained, as shown in figure 15 (sequence on the bottom left). In the same figure, experimental drop contours are also presented (sequence on the bottom right) along the same trajectory. Although the fine details do not match, the occurrence of drop break-up is captured. This is a general result, in the sense that simulations correctly predict whether or not a drop breaks up, as well as the qualitative drop evolution, at different trajectories and/or by varying the rotational speed of the cylinders.

Many other single drop transients have of course been dealt with in the literature, which are not reported here. We just mention as an example the case of oscillatory shear flow [53], which has been tackled from the experimental, numerical, and modelling side. This might be a promising topic, in particular in the situation of large amplitude oscillatory shear (LAOS), which has recently gained popularity as a technique to investigate on the microstructure of complex fluids.

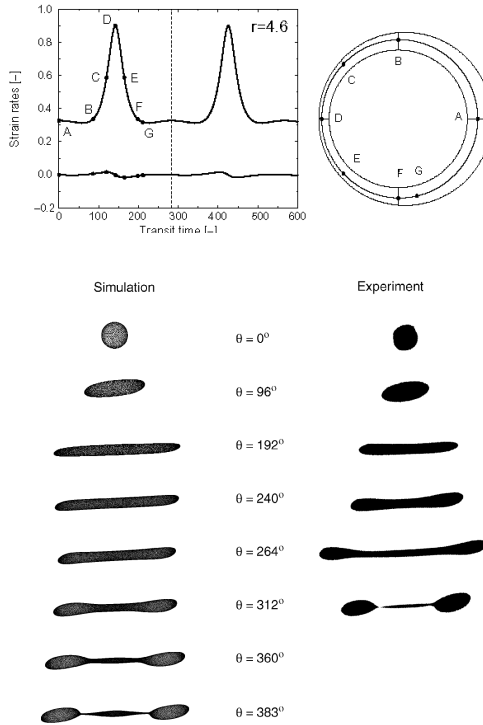


Figure 15: Top: Calculated values of the local elongational and shear rate (left plot) along a trajectory in the eccentric cylinder device (right schematic). Bottom: Calculated (left) and experimental (right) drop contours for an inner cylinder rotation speed of 18 rpm at $\lambda = 2.5$ (adapted from Feigl *et al.* [52]).

3. NON-NEWTONIAN SYSTEMS

3.1 Mathematical Background for the non-Newtonian Case

The fluid-dynamics of the drop problem in the case where one or both the component fluids are viscoelastic is expected to be intricate, as the constitutive time scales of the two fluids also come into play, together with the intrinsic time scale τ_{em} related to the very existence of an interface. It so appears that even the identification of relevant non-dimensional parameters is challenging. In fact, for the non-Newtonian case, the choice of a suitable constitutive equation for the fluids has to be made, which seems to imply that results of general validity cannot be obtained. This situation

changes, however, when “slow flows” only are considered. Indeed, it is well known that slow (and slowly varying) flows imply a *universal* rheological response of the fluid, for the vast category of the so-called “simple fluids”, first introduced by Noll in the 1950s [9, 10]. The resulting universal constitutive equation for the stress tensor \mathbf{T} , namely, the “second-order fluid” constitutive equation, reads:

$$\mathbf{T} = -P\mathbf{I} + 2\eta\mathbf{D} + \beta_{11}\mathbf{D} \cdot \mathbf{D} + \beta_2\mathbf{A} \quad \dots\dots\dots(21)$$

where \mathbf{A} is the second-order Rivlin-Ericksen tensor [9, 10], and the constant constitutive coefficients β_{11} and β_2 are related to normal stresses ($\beta_2 = -N_1/(2\dot{\gamma}^2)$, $\beta_{11} = 4(N_1 + N_2)/\dot{\gamma}^2$, with N_1 and N_2 the first and second normal stress differences, respectively, in shear flow). Thus, although the actual limits of validity of the slow flow assumption may be unknown beforehand, second-order fluid results enjoy a broad applicability, and the effects of constitutive elasticity (the first “deviations” from the Newtonian situation) are now correctly included in the analysis.

The second-order fluid constitutive equation has been adopted recently [54] to perturbatively studying the steady-state drop problem at the highest possible level of generality in the non-Newtonian case. With all the same simplifying assumptions previously stated for the Newtonian situation (isothermal conditions, incompressibility and immiscibility, inertialess dynamics with negligible external and buoyancy forces, constant interfacial tension), and with the same non-dimensionalizations (drop radius R_0 as the unit length, stresses scaled with the interfacial stress σ/R_0), the governing dynamical equations are:

$$\begin{aligned} \nabla \cdot \mathbf{v} &= 0, & -\nabla P + 2\nabla \cdot \mathbf{D} + \frac{\sigma\beta_2}{R_0\eta^2} \nabla \cdot \left(\mathbf{A} + \frac{\beta_{11}}{\beta_2} \mathbf{D} \cdot \mathbf{D} \right) &= \mathbf{0} \\ \nabla \cdot \mathbf{v}_d &= 0, & -\nabla P_d + 2\nabla \cdot \mathbf{D}_d + \frac{\sigma\beta_{2d}}{R_0\eta_d^2} \nabla \cdot \left(\mathbf{A}_d + \frac{\beta_{11d}}{\beta_{2d}} \mathbf{D}_d \cdot \mathbf{D}_d \right) &= \mathbf{0}, \end{aligned} \quad \dots\dots\dots(22)$$

with the interfacial boundary conditions at $F(\mathbf{R},t)=0$:

$$\mathbf{v} = \frac{1}{\lambda} \mathbf{v}_d \quad \dots\dots\dots(23)$$

$$\mathbf{v} \cdot \mathbf{N} = 0 \quad \dots\dots\dots(24)$$

$$N\nabla \cdot \mathbf{N} = \left\{ (P_d - P)\mathbf{I} + 2(\mathbf{D} - \mathbf{D}_d) + \left[\frac{\sigma\beta_2}{R_0\eta^2} \left(\mathbf{A} + \frac{\beta_{11}}{\beta_2} \mathbf{D} \cdot \mathbf{D} \right) - \frac{\sigma\beta_{2d}}{R_0\eta_d^2} \left(\mathbf{A}_d + \frac{\beta_{11d}}{\beta_{2d}} \mathbf{D}_d \cdot \mathbf{D}_d \right) \right] \right\} \cdot \mathbf{N} \quad \dots\dots\dots(25)$$

Boundary conditions “at infinity” are the same as for the Newtonian case: $\mathbf{v} \rightarrow Ca\mathbf{L}^{(\infty)} \cdot \mathbf{r}$ and $P \rightarrow P^{(\infty)}$ as $\mathbf{r} \rightarrow \infty$.

Two new fully constitutive parameters now appear, namely, β_{11}/β_2 and β_{11d}/β_{2d} , which are proportional to the *constant* ratios $\Psi \equiv -N_2/N_1$ and $\Psi_d \equiv -N_{2d}/N_{1d}$, respectively, of the second to the first normal stress differences of the two component fluids. Two further new coefficients also emerge, namely, $p \equiv \sigma\beta_2/(R_0\eta^2)$ and $p_d \equiv \sigma\beta_{2d}/(R_0\eta_d^2)$, pertaining to the fluid pair. These coefficients can be looked at as *ratios of characteristic times*. For example, p is the ratio of the constitutive relaxation time $\Psi_1/2\eta$ of the outer fluid ($\Psi_1 \equiv N_1/\dot{\gamma}^2$) and the interfacial relaxation time $R_0\eta/\sigma \equiv \tau_{em}$.

To further understanding the meaning of p and p_d , we write (e.g., for the outer fluid):

$$p \equiv \frac{\sigma\beta_2}{R_0\eta^2} = \frac{\sigma^2}{R_0^2\eta^2} \frac{\beta_2 \left| \mathbf{L}_{DIM}^{(\infty)} \right|^2}{\left| \mathbf{L}_{DIM}^{(\infty)} \right|^2} \frac{\sigma}{R_0} \equiv \frac{1}{Ca^2} N \quad \dots\dots\dots(26)$$

(Analogously, we will have $p_d \equiv N_d/(\lambda^2 Ca^2)$.) The non-dimensional N defined in equation (26) is the ratio of elastic to interfacial stress, in the same way as the capillary number is the ratio of viscous to interfacial stress. In other words, N is the non-Newtonian counterpart of Ca . We emphasize that N , from its definition in equation (26), is of second order in the flow strength $\left| \mathbf{L}_{DIM}^{(\infty)} \right|$, i.e., elastic effects only show up at second order under steady state conditions, as it must be. Thus, the p parameter is a *measure of the “weight” of constitutive elasticity for the drop problem*, and $p \geq 1$ is the condition to be fulfilled to make non-Newtonian effects observable [54].

It is now apparent from equation (26) how a perturbation procedure can be worked out, by adopting the non-dimensional numbers Ca , N , and N_d as the expansion parameters, in the limit of small drop deformations. Indeed, the conditions of small Ca and N , N_d are seen to imply small deformations of the drop from its unperturbed spherical shape, because interfacial forces are dominant. Double expansion of all fields P , P_d , \mathbf{v} , \mathbf{v}_d , and F in equations (22) to (25) can then be formally written down, and non-Newtonian effects are obtained by solving the mathematical problem at first order in N and N_d (which means at order $\left| \mathbf{L}_{DIM}^{(\infty)} \right|^2$). Notice that, for the drop shape, by adopting the same analysis as for the Newtonian case (i.e., based on rotational invariance and representation theorems), we can immediately write down now:

$$\begin{aligned} \mathbf{R}(\mathbf{u}) = & 1 + Ca\mathbf{T}\mathbf{D}^{(\infty)} : \mathbf{u}\mathbf{u} \\ & + \left[(Ca^2s_1 + Ng_1 + N_dg_{1d}) \mathbf{D}^{(\infty)} \mathbf{D}^{(\infty)} : \mathbf{u}\mathbf{u}\mathbf{u}\mathbf{u} + (Ca^2s_2 + Ng_2 + N_dg_{2d}) \mathbf{D}^{(\infty)} \cdot \mathbf{D}^{(\infty)} : \mathbf{u}\mathbf{u} \right. \\ & \left. + (Ca^2s_3 + Ng_3 + N_dg_{3d}) \mathbf{D}^{(\infty)} : \mathbf{D}^{(\infty)} + (Ca^2s_4 + Ng_4 + N_dg_{4d}) (-\mathbf{W}^{(\infty)} \cdot \mathbf{D}^{(\infty)} + \mathbf{D}^{(\infty)} \cdot \mathbf{W}^{(\infty)}) : \mathbf{u}\mathbf{u} \right] \\ & \dots\dots\dots(27) \end{aligned}$$

i.e., drop shape is again univocally expressed in terms of the flow field at infinity, but the “scalar coefficients” at second order in $|\mathbf{L}_{DIM}^{(\infty)}|$ now depend on the viscosity ratio λ plus the non-Newtonian parameters p , Ψ , p_d , and Ψ_d [54].

No analytic results are presently known for the drop problem with non-Newtonian components when going beyond the small deformation limit. Here, however, at variance with the Newtonian case, numerical simulations have not really been exploited. The reason for this is twofold. On the one hand, the choice of a “realistic” but manageable constitutive equation (among the numerous ones available) is needed, which is not straightforward. On the other hand, in the lack of a powerful “trick” similar to the Boundary Integral representation for the Newtonian case, simulations are perforce fully 3D, hence computationally very heavy. Furthermore, special methods of integration are required, as traditional Finite Element methods have often been found to break down for non-Newtonian flows having even small amounts of viscoelasticity [29]. Thus, only a few simulations of drop deformation with non-Newtonian fluids have in fact been performed, which will be mentioned later in the review, and the field is open to future work.

In such a situation, the quite recent introduction [27] of a phenomenological model for drop dynamics with non-Newtonian fluid components is especially welcome. The model is in the class of the “ellipsoidal models”, discussed above, i.e. where the drop is taken to be ellipsoidal at all times. The dynamics are specified by the simple equation:

$$\begin{aligned} \frac{d\mathbf{Q}}{dt} + (-\mathbf{W}^{(\infty)} \cdot \mathbf{Q} + \mathbf{Q} \cdot \mathbf{W}^{(\infty)}) + a(\mathbf{D}^{(\infty)} \cdot \mathbf{Q} + \mathbf{Q} \cdot \mathbf{D}^{(\infty)}) + b\mathbf{D}^{(\infty)} : \mathbf{Q}\mathbf{I} + c\mathbf{D}^{(\infty)} \text{Tr}(\mathbf{Q}) \\ = -\frac{f}{\tau_{em}} [\mathbf{Q} - g(\mathbf{Q})\mathbf{I}] \end{aligned} \tag{28}$$

(Tr(...) represents the trace operator.) The LHS of equation (28), with a , b , and c arbitrary numbers, expresses the most general symmetry-preserving time derivative of tensor \mathbf{Q} , linear in \mathbf{Q} itself. The RHS of the equation is a simple relaxation term, with g an appropriate volume-preserving function. A determination of the coefficients in equation (28) is obtained, analogously to the Newtonian case, by the expansion of the equation in Ca , and by a comparison of the resulting first- and second-order equations with the exact steady-state solutions for the drop shape (Taylor solution at order Ca , and the complete second-order solution as given in equation (27)). Coefficients a , b , c , and f determined in this way all depend on λ and on the non-Newtonian parameters p , Ψ , p_d , and Ψ_d , and drop dynamics is thereafter fully specified for whatever imposed flow field.

Without actually solving for drop dynamics, we would however like to immediately signal here a notable qualitative prediction of equation (28), for the case of drop relaxation in the absence of externally imposed flows. In such a case, all terms of equation (28) containing the external flow field are switched off, of course, and only the relaxation term in the RHS is active, with a relaxation rate given by f/τ_{em} . Since f will contain the non-Newtonian parameters of the fluid pair, the conclusion is

reached that, no matter how small is the initial deformation of the drop, its relaxation is influenced by the viscoelastic properties of the component fluids [27]. This and other predictions of equation (28) will be discussed in the following, as appropriate.

3.2 Shear flow

As reported in the previous section, the only known analytical solution of our single drop fluid-dynamic problem for non-Newtonian fluids is a steady-state perturbative solution up to second order in Ca , where the two fluid components are second-order fluids [54]. From this solution, in the case of shear flow, the expressions for the observable axes and the angle ϕ (as deduced from equation (27)) are:

$$R_{MAX} = 1 + Ca \frac{16 + 19\lambda}{16(1 + \lambda)} + Ca^2 F(\lambda, p, \Psi, p_d, \Psi_d) \quad \dots\dots\dots(29)$$

$$R_{MIN} = 1 - Ca \frac{16 + 19\lambda}{16(1 + \lambda)} + Ca^2 F(\lambda, p, \Psi, p_d, \Psi_d) \quad \dots\dots\dots(30)$$

$$R_Z = 1 + Ca^2 G(\lambda, p, \Psi, p_d, \Psi_d) \quad \dots\dots\dots(31)$$

$$R_p = 1 + Ca^2 H(\lambda, p, \Psi, p_d, \Psi_d) \quad \dots\dots\dots(32)$$

$$\phi = \frac{\pi}{4} - Ca \left[\frac{(16 + 19\lambda)(3 + 2\lambda)}{80(1 + \lambda)} + p \frac{176 + \lambda(436 + 323\lambda)}{30(1 + \lambda)(16 + 19\lambda)} + p_d \frac{9\lambda^2 + 6\lambda^3}{8(1 + \lambda)^2} \right] \quad \dots\dots\dots(33)$$

Concerning the axes R_{MAX} and R_{MIN} , notice that the second-order coefficient is the same in both equations (29) and (30), just as it was for the Newtonian case. Hence, also in the non-Newtonian case the deformation parameter $D \equiv (R_{MAX} - R_{MIN}) / (R_{MAX} + R_{MIN})$ remains linear in Ca throughout the range of validity of second order theory (see equation (14)), and the interfacial tension σ can again be obtained from side view experiments. Concerning the top view axes R_Z and R_p , again directly quadratic in Ca , it is seen from equations (31) and (32) that a measure of the second order coefficients (through optical means) gives direct information on the rheological properties of the component fluids. Finally, it should be emphasized that fitting of equation (33) to side view optical data of drop orientation leads in fact to a direct determination of the first normal stress difference N_1 of either component fluid, because Ψ and Ψ_d do not appear in the expression of ϕ .

To check these predictions, a proper choice of the fluids to be used in the optical experiments is on demand. Indeed, high elasticity second order fluids (in the range of $\dot{\gamma}$ to be used) are required, in order to have p or p_d of order unity. Model fluids fulfilling these conditions are the well-known Boger fluids [55], which are obtained by adding a small amount of a high molecular weight polymer solution to a sample of the same polymer of quite lower molecular weight, the latter in practice being a Newtonian fluid. In the small deformation experiments to be discussed next [56], the Boger fluids selected as the matrix phase were based on polyisobutylene, with kerosene as a solvent. In the range of shear rates investigated (0.1 to 1 s^{-1}), the

viscosities of each Boger fluid were essentially constant (all of them around 10 Pa·s), and the first normal stress differences were quadratic in $\dot{\gamma}$, with Ψ_1 in the range 3-30 Pa·s². As the drop phase, silicone oils of different viscosity were used, so that λ of the fluid pair could be varied. Since typical drop radius was 50 μm , and σ was around 3 mN/m, it is readily seen that p values ranged from 0.5 to 5, hence significant non-Newtonian effects are expected.

Experimental data obtained through the sliding plate and video microscopy apparatus already described are shown in figures 16 and 17 [56]. In figure 16, side view images of deformed drops under steady shear at the same capillary number and viscosity ratio are also presented, the leftmost one corresponding to a fully Newtonian system, the other to a non-Newtonian case with $p = 4$ (and $p_d = 0$). These images vividly display the stronger alignment of the drop in the flow direction occurring in the non-Newtonian case. The plot in figure 16 compares orientation data with values calculated from equation (33). The large non-Newtonian orientational effect predicted by theory is in excellent agreement with experimental results, thus confirming that normal stresses in the matrix fluid act to align the drop in the shear direction. In figure 17, data and predictions are compared for the projected axis R_p . Non-Newtonian

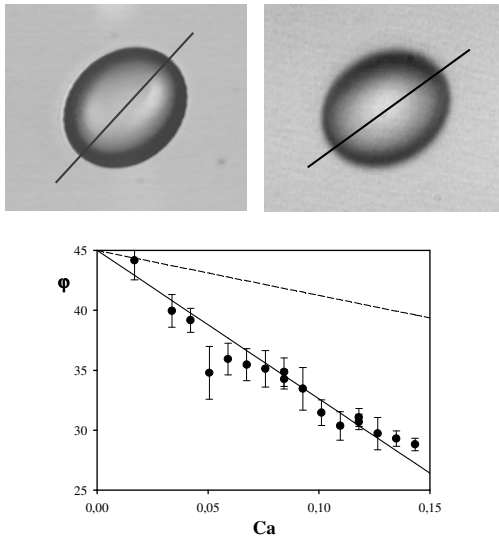


Figure 16: Top: Side view images of deformed drops under steady shear for $p = 0$ (left) and $p = 4$ (right), and at the same Ca ($= 0.15$) and λ ($= 0.1$). Bottom: Plot of drop orientation vs Ca for $p = 4$ and $\lambda = 0.1$ [56]. Continuous line is the theoretical prediction for $p = 4$, dashed line is the Newtonian prediction ($p = 0$).

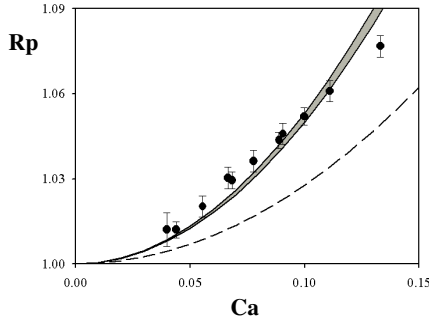


Figure 17: The projected axis R_p vs Ca for $p = 3$ and $\lambda = 0.1$. The gray area encompasses non-Newtonian predictions with varying Ψ .

predictions for $p = 3$ at various Ψ values essentially collapse on each other, thus showing that the second normal stress difference is ineffective in this case. These findings are again confirmed by experiments. It is concluded that side and top view experiments like those in figures 16 and 17, together with predictions from theory, do provide a novel tool to measure the first normal stress difference, at least for highly elastic fluids. Conversely, if N_1 is known, the interfacial tension can be determined.

In a recent paper, in dealing with a (quasi) Newtonian drop in a Boger fluid, Mighri *et al.* [57] found a marked positive deviation of R_p from the Newtonian case, in qualitative agreement with the just presented results, but interpreted this effect as an increase in drop deformation due to matrix elasticity. It should be mentioned in this respect that shear experiments in [57] were carried out by using two transparent parallel disks mounted on a Weissenberg rheogoniometer, so only observations along the velocity gradient were feasible. Thus, it was not possible to discriminate between a true and an apparent increase in drop deformation, the latter being actually due to an increase in drop orientation, as shown in figure 16 [56]. It is then clear that a complete characterization of drop shape requires observations from different views. This same conclusion is reached when dealing with the reverse problem of a Boger fluid drop in a Newtonian matrix. In this situation, Mighri *et al.* found a negative deviation of R_p from the Newtonian case. On the other hand, from equation (33), drop orientation towards the shear direction is predicted to increase in this inverse situation, too. These two findings cannot at present be reconciled, and further experiments are surely needed.

At higher capillary numbers, i.e., outside the small deformation limit, the scenario is not well defined, since data of drop deformation are rather sparse, and systematic investigations by varying deformation rates and fluid constitutive parameters are lacking. The only point where some kind of general picture seems to emerge from literature is drop break-up under flow. As early as in 1972, Flumerfelt [58] reported experimental results on break-up of Newtonian drops in shear flows of

viscoelastic fluids. He found that all data of critical shear rate $\dot{\gamma}_{cr}$ were well represented by the simple equation:

$$Ca_{cr} \equiv \frac{R_0 \eta(\dot{\gamma} \rightarrow 0) \dot{\gamma}_{cr}}{\sigma} = \kappa \left(\frac{\eta_d}{\eta(\dot{\gamma} \rightarrow 0)} \right) \tau \dot{\gamma}_{cr} + Ca_{cr}^{(Newt)} \quad \dots\dots\dots(34)$$

In this equation, τ is the main relaxation time and $\eta(\dot{\gamma} \rightarrow 0)$ the zero shear viscosity of the viscoelastic matrix fluid, $\lambda_0 \equiv \eta_d / \eta(\dot{\gamma} \rightarrow 0)$ is the zero shear viscosity ratio, and $Ca_{cr}^{(Newt)}$ is the critical capillary number of a fully Newtonian system with the same viscosities. Since it is found $\kappa(\lambda_0) > 0$, from equation (34) it follows that i) the non-Newtonian critical capillary number is always larger than the corresponding Newtonian one, and ii) $R_0 > \tau \sigma \kappa(\lambda_0) / \eta(\dot{\gamma} \rightarrow 0)$, i.e. there exists a minimum drop size below which break-up cannot be achieved. It should be immediately mentioned here that point i) was later confirmed in the reverse case (non-Newtonian drop in a Newtonian matrix) by Varanasi *et al.* [59], hence it seems to be a general, robust result. On the other hand, the existence of a minimum radius for break-up (point ii) is better seen as a result limited to the range of shear rates investigated by those authors, as it will be specified below.

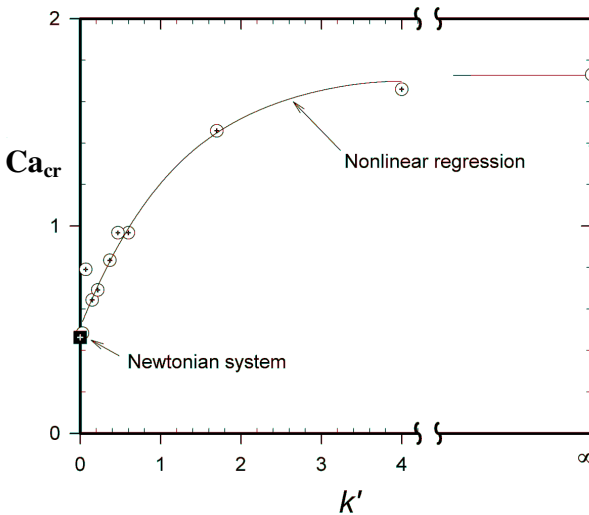


Figure 18: The critical capillary number Ca_{cr} as a function of the “elasticity ratio” $k' \equiv \tau_d / \tau$ under shear flow for Boger fluid pairs [57].

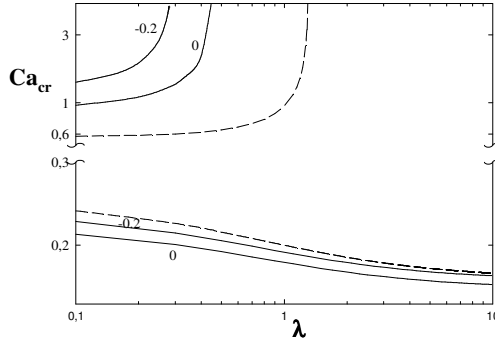


Figure 19: Ellipsoidal model predictions of the critical capillary number as a function of the viscosity ratio, for $p = 1$ [27]. Dashed lines are the Newtonian prediction, continuous lines are the non-Newtonian predictions at different Ψ values.

In the drop break-up experiments described so far, the non-Newtonian behaviour of the fluids investigated included both viscosity shear-thinning and less than quadratic normal stresses. In other words, it so happened in these experiments that “high” non-dimensional shear rates were at play, i.e., with $\tau\dot{\gamma} > 1$. Hence, a clear identification of separate elastic and viscous non-Newtonian effects was in fact not achieved. By using Boger fluids, conversely, it is expected that this difficulty can be overcome, also because of the absence of any shear-thinning. Mighri *et al.* [57] used many pairs of Boger fluids to study break-up conditions with different drop to matrix elasticity ratios, as expressed by $k' = \tau_d / \tau$. In figure 18, from their work, the variation of the critical capillary number Ca_{cr} with the elasticity ratio k' is reported. The data points in figure 18, however, correspond to fluid pairs with different values of viscosity ratio λ , p and p_d (and, of course, of k'). We found that the range of λ was rather limited (0.3 – 1.1), but that p and p_d span at least an order of magnitude. In this respect, the non-linear regression shown by the authors is of difficult interpretation. Nevertheless, the general statement, that drop break-up is inhibited by elastic effects, remains true.

In figure 19, the critical capillary number Ca_{cr} at break-up is calculated as a function of the viscosity ratio (and both for shear and elongational flow) from the only available ellipsoidal model dealing with non-Newtonian fluid components [27]. Only the case of a Newtonian drop in a non-Newtonian matrix is shown. Top curves correspond to shear break-up with $p = 1$ and $p_d = 0$, and the dashed curve refers to the fully Newtonian system. Model predictions are in line with the experimental observations of an elasticity-induced increase of Ca_{cr} with respect to the Newtonian case. An interesting result here concerns the large calculated effect of the Ψ parameter, i.e., of the second normal stress difference. Although quantitative agreement with

break-up data is not expected in general for any ellipsoidal model, the predicted trend with varying Ψ might be observable and awaits experimental validation.

In the part on fully Newtonian systems, we have already described the drop widening along the vorticity axis, which precedes break-up at very high capillary numbers. This phenomenon was actually first observed by Levitt *et al.* [50] in non-Newtonian polymer blends in the molten state, by using two transparent counter-rotating parallel disks to shear the samples. Both components (polypropylene for the drops and polystyrene for the matrix) were highly elastic. Drop widening was only observed (at a fixed $\dot{\gamma} = 1 \text{ s}^{-1}$) when the matrix was more elastic than the drop phase. Based on this finding, Levitt *et al.* proposed an explanation of the widening effect as due to the second normal stress difference of the matrix fluid. On the other hand, we calculate that the non-dimensional elasticity parameter p in their systems is quite low, because of the high viscosity of polymer melts. Since the true measure of elasticity in the drop-in-a-fluid system is the p parameter, we argue that the effect observed by Levitt *et al.* is not necessarily linked to the non-Newtonian character of the fluids employed.

We finally signal that, quite recently, top view observations of completely new modes of deformation and break-up along the vorticity axis of shear flow have been independently reported by Migler [60] and by Mighri and Huneault [61]. In both these works, Boger fluids based on polyisobutylene were used for the drops, and the matrix was a Newtonian polydimethylsiloxane. The viscosity ratio was around unity, and $2 < p_d < 4$. The imposed shear rates were quite large (up to ca. 100 s^{-1}), with correspondingly large capillary numbers. Migler used a parallel disk apparatus coupled to stroboscopic optical microscopy to capture images of the fast moving drops. On the other hand, Mighri and Huneault used a transparent Couette cylindrical counter-rotating flow cell in order to keep the deformed drop in a stationary plane of view. In figure 20 (from [61]), a sequence of images showing steady state drop shapes at increasing capillary numbers is presented in the left panel. The sequence illustrates how, by increasing Ca , the usual drop elongation along the flow direction is at some point reversed, and replaced by an elongation along the vorticity axis. In the right panel of the same figure, the evolution in time of drop shape is shown, taking place at a much higher capillary number, and a break-up in the vorticity direction is in the end observed. Both the steady state and the transient phenomena just described lack a clear interpretation, and further work is definitely needed.

3.3 Elongational flow

Although an analytic solution for elongational flows in the non-Newtonian case exists in the limit of small deformations [54], we are not aware of any data to be compared with theoretical predictions. In fact, the few available data pertain to a range of moderate to large drop deformations, some of them up to break-up. The non-Newtonian ellipsoidal model [27] is then the adequate tool to be used for data interpretation, together with the few existing numerical simulations, which are however limited to the uniaxial case only.

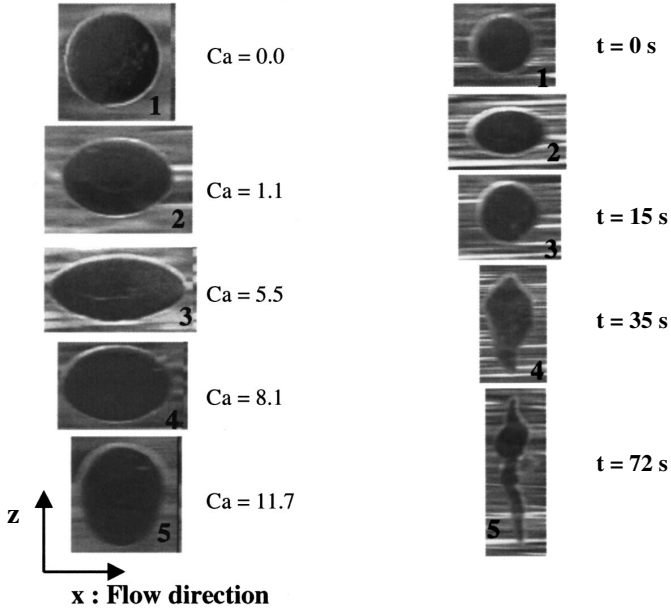


Figure 20: Images of viscoelastic drops sheared in a Newtonian matrix ($\lambda = 1.3$). Left panel: steady state drop shapes at increasing capillary numbers. Right panel: a sequence showing the time evolution of drop shape at a supercritical capillary number [61].

Let us start with the planar elongational case. In figure 21, deformation parameter data of Newtonian drops of different radii elongated in a polyisobutylene-based suspending Boger fluid are plotted, as a function of the capillary number. These data are from a recent paper by Trethewey and Leal [62], and correspond to a viscosity ratio around unity; empty symbols refer to the equivalent fully Newtonian system, i.e., with the same viscosity ratio. It is seen that data exhibit an upward deviation with respect to the Newtonian case, the more so the smaller is drop radius. This trend is expected, since elastic effects are predicted to increase with decreasing drop radius, on the basis of the p parameter, $p = \Psi_1 \sigma / (2R_0 \eta^2)$. Thus, drop deformation depends on drop size (through p), at variance with the Newtonian case. The lines in figure 21 are the predictions of the non-Newtonian ellipsoidal model [27], which are found in good qualitative agreement with data, at least when the deformation parameter is not too large. Concerning break-up, both experiments and predictions indicate that elasticity makes the drops easier to break when the external fluid is elastic (see figure 19), the reverse being true for the case of an elastic drop [63].

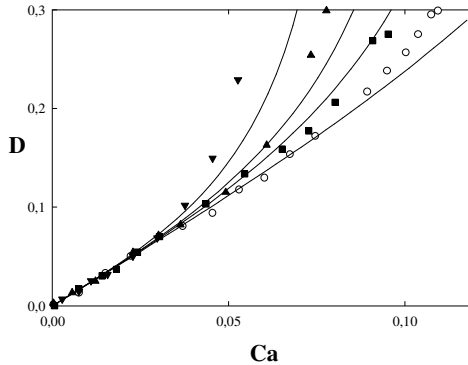


Figure 21: The deformation parameter vs Ca for a Newtonian drop in a viscoelastic matrix under planar elongational flow at $\lambda = 1.08$. Data from [62], continuous lines from [27]. p increases from bottom to top.

As mentioned in the theoretical section, an interesting feature to be investigated is the possible effect of the non-Newtonian character of the fluid components on drop relaxation upon cessation of flow. In figure 22, a comparison of the relaxation of a Newtonian drop in a Newtonian and a non-Newtonian Boger fluid is presented [39], for the same viscosity ratio. The drop in the viscoelastic fluid retracts much more slowly than the drop in the Newtonian fluid. Such a slowing down effect is captured by the non-Newtonian ellipsoidal model [27], even though the upward curvature of the relaxation curve is not. It should be noticed that the p parameter pertaining to the experimental data shown in figure 22 is quite high (much larger than 10 according to Ha and Leal), hence the effect on relaxation is quite pronounced. It seems worth emphasizing again here that the parameter p (and p_d) contains the drop radius, hence systems having the same non-Newtonian constitutive properties, but with drops of different size, exhibit different relaxations. It is then important to account for this aspect when interfacial tension is measured by means of drop retraction in non-Newtonian systems.

Drop dynamics in the non-Newtonian case remains quite complex, and still largely unexplored. In figure 23, an example of transient drop deformation during start-up of planar elongational flow is shown [62]. The data in figure 23 refer to four different capillary numbers, consecutively imposed (restarting from rest) on the same drop. During time evolution of the deformation parameter, a pseudo steady state plateau is reached, followed by a sharp increase with an overshoot before attaining the true steady state condition. This transient behaviour is most likely linked to elasticity, as expressed by the p parameter, which is here around 10. This interpretation is confirmed by the finding that, when the same experiment was repeated for a larger drop size (hence, for a smaller p), no such complex time evolution was observed [62].

It should be mentioned that the non-Newtonian ellipsoidal model does not predict such dynamics. Needless to say, still more complex dynamics are found for “realistic” elongational flow fields [64, 65].

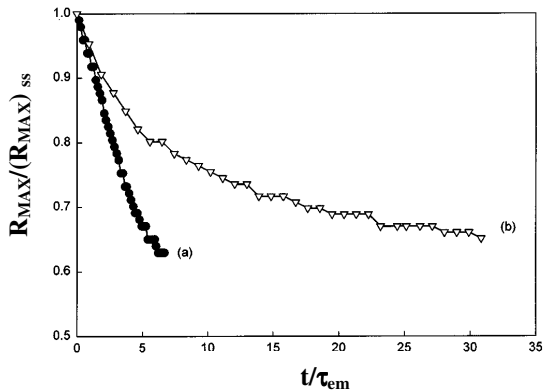


Figure 22: . The deformation parameter during relaxation of a Newtonian drop in a Newtonian (a) and a non-Newtonian Boger fluid (b), [39].

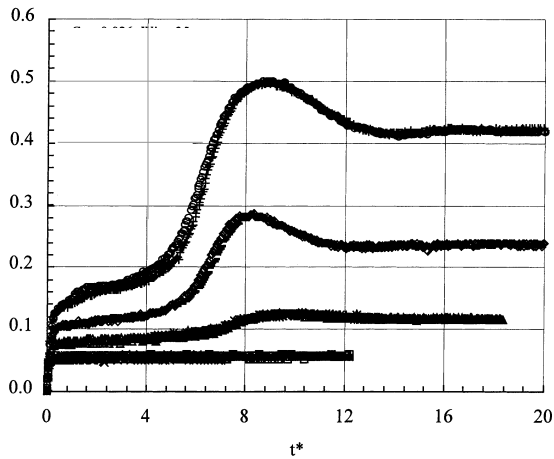


Figure 23: Transient drop deformation during start-up of planar elongational flow at $\lambda = 0.42$ (p around 10) and at four capillary numbers (from 0.026 to 0.065). Adapted from [62].

Finally, going to the uniaxial elongational case, we stress again that the only available data are from Delaby *et al.* [30], which have been already discussed in the part referring to Newtonian systems. Here, it is worth mentioning that Delaby *et al.* [66], in an attempt of interpreting their data, used the Palierne model of linear viscoelasticity [67]. Good agreement between experiments and predictions was found, but this outcome is not easily understood, since Palierne analytic model only deals with small drop deformations, whereas data correspond to intermediate to large deformations. We believe that further understanding should rather come either from theories not limited to the small deformation range or from suitable numerical simulations.

In fact, the few available numerical simulations for the drop problem with non-Newtonian fluid components are for the uniaxial elongation case, where symmetry can be exploited to drastically simplify the calculations. It should be mentioned that, in these simulations, the choice of the constitutive equation of the fluid components is to some extent arbitrary, and is then dictated mainly by mathematical convenience. Concerning steady state, results are limited to modest drop deformations, and show that slightly more pointed shapes with respect to the fully Newtonian case are obtained, when the suspending fluid is viscoelastic [68]. Some interesting features emerge from transient situations. Upon inception of flow, drop deformation overshoots are calculated [29], which are small, however, at least in the range of extension rates examined. During recovery upon cessation of flow, the above described slowing down of drop retraction is also found in numerical simulations [28]. Another notable result is that, after stopping the extensional elongation, a drop in a viscoelastic matrix can exhibit a significant lengthening before retraction, in a way strongly dependent on how the flow is stopped [28]. It so appears that the study of drop deformation through numerical simulations in the non-Newtonian case is promising, but still in its early stage.

4. CONCLUSIONS

The panorama delineated in this review shows how the single drop problem constitutes an active area of ongoing research, where novel results continue to appear, both on the experimental and the theoretical side. Having in mind our perspective of what happened in the last decade, what can we learn from the works reported in the literature and here summarized?

An important result of immediate practical application surely is the development of methods to measure the interfacial tension, which is the most relevant physical parameter in multiphase systems. These methods, rooted in the fluid-dynamics of the single drop, allow one to determine values of interfacial tension spanning several orders of magnitude, including extreme situations (e.g., for very high or very low viscosities [69]) where difficulties are experienced with classical measuring methods. Furthermore, some of these methods, based on stationary drop shapes in the small deformation limit, can be applied both in case of fully Newtonian and non-Newtonian systems.

Concerning rheometrical aspects, it should be emphasized how the single drop system in flow can be regarded as an “optical micro-rheometer”, which can be used to measure viscoelastic fluid properties with tiny quantities of material. For the Newtonian case, this opportunity, though in fact already implicit in the seminal work of Taylor, has been exploited only recently for viscosity measurements [70]. In the non-Newtonian case, recent theoretical developments showing a link between drop orientation and elastic stresses afford a relatively simple experimental route to optically measure the first normal stress difference N_1 , i.e., one of the most relevant viscoelastic material property.

Another important phenomenon where our understanding has significantly improved in the last ten years is drop break-up under flow. This may be also of practical relevance, as it opens the way to the study of post-break-up morphology, e.g., the number and distribution of daughter drops. In very broad terms, one might then argue that a better comprehension of mixing is in view. However, some caution seems at order at this stage. In fact, in concentrated systems of practical relevance, drop-drop interactions (including coalescence) play a prominent role, and the transposition of single drop results to multi-drop situations is not warranted. In one of the best-known models of concentrated liquid-liquid systems, i.e., the Doi-Ohta model [71], drops disappear at all, as it actually occurs in co-continuous morphologies, and the attention is shifted to the interface as the appropriate dynamical object.

Going back to the “simple” single drop problem, perspectives of future work can be anticipated in several areas. A first example is the study of the effects of surfactants on drop deformation and dynamics. It is well known that small amounts of surface active agents do lead to significant alterations with respect to the “clean” interface situation [72], a response that can be advantageously used in the design of liquid-liquid suspensions. Another example is the investigation of how the behaviour of the deforming drop is affected by the viscoelastic properties of “realistic” non-Newtonian fluids (as opposed to model fluids), such as shear thinning viscosity or normal stresses. It should also be stressed that experiments on and modelling of drop deformation in complex flow fields, such as the ones encountered in processing, are strongly on demand. We conclude that the drop-in-a-flow-field problem still represents a fascinating and fertile subject.

REFEREENCES

1. Han C D, “Multiphase flow in polymer processing”. Academic (London), (1981).
2. Larson R G, “The Structure and Rheology of Complex Fluids”, Oxford University Press (New York), (1999).
3. Taylor G I, “The viscosity of a fluid containing small drops of another fluid”, *Proc. R. Soc. London A*, 138 (1932) 41-48.
4. Taylor G I, “The formation of emulsions in definable fields of flow”, *Proc. R. Soc. London A*, 146 (1934) 501-523.

5. Rallison J M, "The deformation of small viscous drops and bubbles in shear flows", *Ann. Rev. Fluid Mech.*, 16 (1984) 45-66.
6. Stone H A, "Dynamics of drop deformation and break-up in viscous fluids", *Ann. Rev. Fluid Mech.*, 26 (1994) 65-102.
7. Tucker III C L and Moldenares P, "Microstructural evolution in polymer blends", *Ann. Rev. Fluid Mech.*, 34 (2002) 177-210.
8. Landau L D and Lifshitz E M, "Fluid Mechanics", Pergamon Press (Oxford), (1959).
9. Astarita G and Marrucci G, "Principles of Non-Newtonian Fluid Mechanics", McGraw-Hill (Maidenhead), (1974).
10. Joseph D D, "Fluid Mechanics of Viscoelastic Liquids", Springer-Verlag (New York), (1990).
11. Barthes-Biesel D and Acrivos A, "Deformation and burst of a liquid droplet freely suspended in a linear shear field", *J. Fluid Mech.*, 61 (1973) 1-21.
12. Rallison J M, "Note on the time-dependent deformation of a viscous drop which is almost spherical", *J. Fluid Mech.*, 98 (1980) 625-633.
13. Greco F., "Second-order theory for the deformation of a Newtonian drop in a stationary flow field", *Phys. Fluids*, 14 (2002) 946-954.
14. Rallison J M and Acrivos A, "A numerical study of the deformation and burst of a viscous drop in an extensional flow", *J. Fluid Mech.*, 89 (1978) 191-200.
15. Kennedy M R, Pozrikidis C and Skalak R, "Motion and deformation of liquid drops, and the rheology of dilute emulsions in simple shear flow", *Computers Fluids*, 23 (1994) 251-78.
15. Maffettone P L and Minale M, "Equation of change for ellipsoidal drops in viscous flow", *J. Non-Newtonian Fluid Mech.*, 78 (1998) 227-241.
16. Jackson N E and Tucker III C L, "A model for large deformation of an ellipsoidal droplet with interfacial tension", *J. Rheol.*, 47 (2003) 659-682.
17. Yu W and Bousmina M, "Ellipsoidal model for droplet deformation in emulsions", *J. Rheol.*, 47 (2003) 1011-1039.
18. Gonzales R C and Woods R E, "Digital image processing", Addison-Wesley (Reading, MA), (1992).
19. Torza S, Cox R G and Mason R G, "Particle motion in sheared suspensions. XXVII. Transient and steady deformation and burst of liquid drops," *J. Colloid Interface Sci.*, 38 (1972) 395-411.
20. Guido S and Villone M, "Three dimensional shape of a drop under simple shear flow", *J. Rheology*, 42 (1998) 395-415.
21. Guido S and Greco F, "Drop shape under slow steady shear flow and during relaxation. Experimental results and comparison with theory", *Rheol. Acta*, 40 (2001) 176-184.

22. Uijttewaal W S J and Nijhof E J, "The motion of a droplet subjected to linear shear flow including the presence of a plane wall," *J. Fluid Mech.*, (1995) 302 45-63.
23. Cristini V, Blawdziewicz J and Loewenberg M, "An Adaptive Mesh Algorithm for Evolving Surfaces: Simulations of Drop Break-up and Coalescence", *J. Comput. Phys.*, 168 (2001) 445-463.
24. Bentley B J and Leal L G, "An experimental investigation of drop deformation and break-up in steady, two-dimensional linear flows", *J. Fluid Mech.*, 167 (1986) 241-283.
25. Hu Y T and Lips A, "Transient and steady state three-dimensional drop shapes and dimensions under planar extensional flow", *J. Rheol.*, 47 (2003) 349-369.
26. Maffettone P L and Greco F, "An ellipsoidal drop model for single drop dynamics with non-Newtonian fluids", *J. Rheol.*, 48 (2004) 83-100.
27. Hooper R W, de Almeida V F, Macosko C W and Derby J J, "Transient polymeric drop extension and retraction in uniaxial extensional flows", *J. Non-Newtonian Fluid Mech.*, 98 (2001) 141-168.
28. Hooper R W, Toose M, Macosko C W and Derby J J, "A comparison of boundary element and finite element methods for modeling axisymmetric polymeric drop deformation", *Int. J. Numer. Meth. Fluids*, 37 (2001) 837-864.
29. Delaby I, Ernst B and Germain Y, "Droplet deformation in polymer blends during uniaxial elongational flow: influence of viscosity ratio for large capillary numbers", *J. Rheol.*, (1994) 38 1705-1720.
30. Grace H P, "Dispersion phenomena in high viscosity immiscible fluid systems and application of static mixers as dispersion devices in such systems," *Chem. Eng. Commun.*, 14 (1982) 225-277.
31. de Bruijn R A, "Deformation and break-up of drops in simple shear flows," PhD thesis, Technische Universiteit Eindhoven, (1989).
32. Lister J R and Stone H A, "Capillary break-up of a viscous thread surrounded by another viscous fluid", *Phys. Fluids*, 10 (1998) 2758-2763.
33. Navot Y, "Critical behaviour of drop break-up in axisymmetric viscous flow", *Phys. Fluids* 11 (1999) 990-996.
34. Cristini V, Guido S, Alfani A, Blawdziewicz J and Loewenberg M, "Drop break-up and fragment size distribution in shear flow", *J. Rheol.*, 47 (2003) 1283-1298.
35. Blawdziewicz J, Cristini V and Loewenberg M, "Critical behaviour of drops in linear flows. I. Phenomenological theory for drop dynamics near critical stationary states", *Phys. Fluids*, 14 (2002) 2709-2718.
36. Li J, Renardy Y Y and Renardy M, "Numerical simulation of break-up of a viscous drop in simple shear flow through a volume-of-fluid method", *Phys. Fluids*, 12 (2000) 269-282.

37. Clark A T, Lal M, Ruddock J N and Warren P B, "Mesoscopic Simulation of Drops in Gravitational and Shear Fields", *Langmuir*, 16 (2000) 6342-6350.
38. Ha J-W and Leal L G, "An experimental study of drop deformation and break-up in extensional flow at high capillary number", *Phys. Fluids*, 13 (2001) 1568-1576.
39. Cohen A and Carriere C J, "Analysis of a retraction mechanism for imbedded polymeric fibres", *Rheol. Acta*, 28 (1989) 223-232.
40. Tjahjadi M, Ottino J M and Stone H A, "Estimating interfacial tension via relaxation of drop shapes and filament break-up", *AIChE J.*, 40 (1994) 385-394.
41. Tomotika S, "On the stability of a cylindrical thread of a viscous liquid surrounded by another viscous fluid", *Proc. R. Soc. London Ser. A*, 150 (1935) 322-337.
42. Elemans P H M, Janssen J M H and Meijer H E H, "The measurement of interfacial tension in polymer/ polymer systems: The breaking thread method", *J. Rheol.*, 34 (1990) 1311-1325.
43. Yamane H, Takahashi M, Hayashi R, Okamoto K, Kashihara H and Masuda T, "Observation of deformation and recovery of poly(isobutylene) droplet in a poly(isobutylene)/ poly(dimethyl siloxane) blend after application of step shear strain", *J. Rheol.*, 42 (1998) 567-580.
44. Almusallam A S, Larson R G and Solomon M J, "A constitutive model for the prediction of ellipsoidal droplet shapes and stresses in immiscible blends", *J. Rheol.*, 44 (2000) 1055-1083.
45. Luciani A, Champagne M F and Utracki L A, "Interfacial tension coefficient from the retraction of ellipsoidal drops", *J. Polym. Sci. Phys. Ed.*, 35 (1997) 1393-1403.
46. Guido S and Villone M, "Measurement of interfacial tension by drop retraction analysis", *J. Colloid Interface Sci.*, 209 (1999) 247-250.
47. Sigillo I, di Santo L, Guido S and Grizzuti N, "Comparative measurements of interfacial tension in a model polymer blend", *Polymer Eng. Sci.*, 37 (1997) 1540-1549.
48. Xing P, Bousmina M and Rodrigue D, "Critical experimental comparison between five techniques for the determination of interfacial tension in polymer blends: Model system of polystyrene/polyamide-6", *Macromolecules*, 33 (2000) 8020-8034.
49. Levitt L, Macosko C W and Pearson S D, "Influence of normal stress difference on polymer drop deformation", *Polymer Eng. Sci.*, 36 (1996) 1647-1655.
50. Cristini V, Hooper R W, Macosko C W, Simeone M and Guido S, "A numerical and experimental investigation of lamellar blend morphologies", *Ind. Eng. Chem. Res. Des.*, 41 (2002) 6305-6311.

51. Feigl K, Kaufmann S F M, Fischer P and Windhab E J, "A numerical procedure for calculating droplet deformation in dispersing flows and experimental verification", *Chem. Eng. Sci.*, 58 (2003) 2351-2363.
52. Wannaborworn S, Mackley M R and Renardy Y, "Experimental observation and matching numerical simulation for the deformation and break-up of immiscible drops in oscillatory shear", *J. Rheol.*, 46 (2002) 1279-1293.
53. Greco F., "Drop deformation for non-Newtonian fluids in slow flows", *J. Non-Newt. Fluid Mech.*, 107 (2002) 111-131.
54. Boger D V and Binnington R, "Separation of elastic and shear thinning effects in the capillary rheometer", *Trans. Soc. Rheol.*, 21 (1977) 515-34.
55. Guido S, Simeone M and Greco F, "Deformation of a Newtonian drop in a viscoelastic matrix under steady shear flow. Experimental validation of slow flow theory", *J. Non-Newtonian Fluid Mech.*, 114 (2003) 65-82.
56. Mighri F, Carreau P J and Aji A, "Influence of elastic properties on drop deformation and break-up in shear flow", *J. Rheol.*, 42 (1998) 1477-1490.
57. Flumerfelt R W, "Drop break-up in simple shear fields of viscoelastic fluids", *Ind. Eng. Chem. Fundam.*, 11 (1972) 312-318.
58. Varanasi P P, Ryan M E and Stroeve P, "Experimental study on the break-up of model viscoelastic drops in uniform shear flow", *Ind. Eng. Chem. Res.*, 33 (1994) 1858-66.
59. Migler K B, "Droplet vorticity alignment in model polymer blends", *J. Rheol.*, 44 (2000) 277-290.
60. Mighri F and Huneault M A, "Dispersion visualization of model fluids in a transparent Couette flow cell", *J. Rheol.*, 45 (2001) 783-797.
61. Tretheway D C and Leal L G, "Deformation and relaxation of Newtonian drops in planar extensional flows of a Boger fluid", *J. Non-Newtonian Fluid Mech.*, 99 (2001) 81-108.
62. Tretheway D C and Leal L G, "Surfactant and viscoelastic effects on drop deformation in 2-D extensional flow", *AIChE J.*, 45 (1999) 929-937.
63. Gonzalez-Nunez R, Chan Man Fong C F, Favis B D and De Kee D, "Deformation of drops in extensional viscoelastic flow", *J. Appl. Polym. Sci.*, 62 (1996) 1627-1634.
64. Mighri F, Aji A and Carreau P J, "Influence of elastic properties on drop deformation and break-up in shear flow", *J. Rheol.*, 42 (1998) 1477-1490.
65. Delaby I, Ernst B, Germain Y and Muller R, "Droplet deformation during elongational flow in blends of viscoelastic fluids. Small deformation theory and comparison with experimental results", *Rheol. Acta*, 34 (1995) 525-533.
66. Palierne J F, "Linear rheology of viscoelastic emulsions with interfacial tension", *Rheol Acta*, 29 (1990) 204-214.

67. Ramaswamy S and Leal L G, "The deformation of a Newtonian drop in the uniaxial extensional flow of a viscoelastic liquid", *J. Non-Newtonian Fluid Mech.*, 88 (1999) 149-172.
68. Wolf B, Frith W J, Singleton S, Tassieri M and Norton I T, "Shear behaviour of biopolymer suspensions with spheroidal and cylindrical particles", *Rheol. Acta*, 40 (2001) 238-247.
69. Hu Y T and Lips A, "Determination of viscosity from drop deformation", *J. Rheol.*, 45 (2001) 1453-1463.
70. Doi M and Ohta T, "Dynamics and rheology of complex interfaces. I", *J. Chem. Phys.*, 95 (1991) 1242-1248.
71. Stone H A and Leal L G, "The effects of surfactants on drop deformation and break-up", *J. Fluid Mech.*, 220 (1990) 161-86.